



# The important contribution of secondary formation and biomass burning to oxidized organic nitrogen (OON) in a polluted urban area: insights from in situ measurements of a chemical ionization mass spectrometer (CIMS)

Yiyu Cai<sup>1,2,3,4,5,★</sup>, Chenshuo Ye<sup>6,★</sup>, Wei Chen<sup>1,2,3,4,5</sup>, Weiwei Hu<sup>1,2,3,4</sup>, Wei Song<sup>1,2,3,4</sup>, Yuwen Peng<sup>7,8</sup>, Shan Huang<sup>7,8</sup>, Jipeng Qi<sup>7,8</sup>, Sihang Wang<sup>7,8</sup>, Chaomin Wang<sup>7,8</sup>, Caihong Wu<sup>7,8</sup>, Zelong Wang<sup>7,8</sup>, Baolin Wang<sup>9</sup>, Xiaofeng Huang<sup>10</sup>, Lingyan He<sup>10</sup>, Sasho Gligorovski<sup>1,2,3,4</sup>, Bin Yuan<sup>7,8</sup>, Min Shao<sup>7,8</sup>, and Xinming Wang<sup>1,2,3,4</sup>

<sup>1</sup>State Key Laboratory of Organic Geochemistry, Guangzhou Institute of Geochemistry, Chinese Academy of Sciences, Guangzhou 510640, China

<sup>2</sup>CAS Center for Excellence in Deep Earth Science, Guangzhou 510640, China

<sup>3</sup>Guangdong-Hong Kong-Macao Joint Laboratory for Environmental Pollution and Control, Guangzhou Institute of Geochemistry, Chinese Academy of Science, Guangzhou 510640, China

<sup>4</sup>Guangdong Provincial Key Laboratory of Environmental Protection and Resources Utilization, Chinese Academy of Science, Guangzhou 510640, China

<sup>5</sup>University of Chinese Academy of Sciences, Beijing 100049, China

<sup>6</sup>Joint Lab for Atmospheric Photochemistry, Guangdong Provincial Academy of Environmental Science, Guangzhou 510045, China

<sup>7</sup>Institute for Environmental and Climate Research, Jinan University, Guangzhou 511443, China

<sup>8</sup>Guangdong-Hongkong-Macau Joint Laboratory of Collaborative Innovation for Environmental Quality, Guangzhou 511443, China

<sup>9</sup>School of Environmental Science and Engineering, Qilu University of Technology, Jinan 250353, China

<sup>10</sup>Key Laboratory for Urban Habitat Environmental Science and Technology, School of Environment and Energy, Peking University Shenzhen Graduate School, Shenzhen 518055, China

★These authors contributed equally to this work.

**Correspondence:** Weiwei Hu (weiwei.hu@gig.ac.cn) and Bin Yuan (byuan@jnu.edu.cn)

Received: 5 January 2023 – Discussion started: 16 January 2023

Revised: 30 May 2023 – Accepted: 18 June 2023 – Published: 9 August 2023

**Abstract.** To investigate the sources and formation mechanism of oxidized organic nitrogen (OON), field measurements of OON were conducted using an iodide-adduct chemical ionization mass spectrometer equipped with a Filter Inlet for Gases and AEROSOLS (FIGAERO-CIMS) during fall of 2018 in the megacity of Guangzhou, China. Using levoglucosan as a tracer of biomass burning emissions, the results show that biomass burning ( $49 \pm 23\%$ ) and secondary formation ( $51 \pm 23\%$ ) accounted for comparable fractions to the total particle-phase OON (pOON) but  $24 \pm 25\%$  and  $76 \pm 25\%$  to the gas-phase OON (gOON), respectively, signifying the important contribution of biomass burning to pOON and secondary formation to gOON in this urban area. Calculations of production rates of gOON indicated that hydroxyl radical (42%) and nitrate radical ( $\text{NO}_3$ ) (49%) oxidation pathways potentially dominated the secondary formation of gOON. A high concentration of  $\text{NO}_3$  radicals during the afternoon was observed, demonstrating that the daytime  $\text{NO}_3$  oxidation might be more important than the previous recognition. Monoterpenes, found to be major precursors of secondary gOON, were mainly from anthropogenic emissions in this urban area. The ratio of secondary pOON to  $\text{O}_x$  ( $[\text{O}_x] = [\text{O}_3] + [\text{NO}_2]$ ) increased as a function of relative humidity and aerosol surface area, indicating that heterogeneous reaction might be an

important formation pathway for secondary pOON. Finally, the highly oxidized gOON and pOON with 6 to 11 oxygen atoms were observed, highlighting the complex secondary reaction processes of OON in the ambient air. Overall, our results improve the understanding of the sources and dynamic variation of OON in the urban atmosphere.

## 1 Introduction

Oxidized organic nitrogen (OON, including organic nitrates – ONs – and nitroaromatics), acting as an important reservoir of atmospheric nitrogen oxides ( $\text{NO}_x = \text{NO} + \text{NO}_2$ ) (Fisher et al., 2016; Romer Present et al., 2020; Romer et al., 2016; Ditto et al., 2022), substantially influences  $\text{NO}_x$  cycling, formation of ozone ( $\text{O}_3$ ) (Farmer et al., 2011; Perring et al., 2013) and secondary organic aerosol (SOA) (Lee et al., 2016; Rollins et al., 2012), thus affecting air quality, climate and ecosystem nutrient cycling (Kiendler-Scharr et al., 2016; Pye et al., 2015). A comprehensive and in-depth understanding of dynamic variations of in situ OON (including in the gas phase – gOON – and the particle phase – pOON) and their sources is crucial for accurately assessing their environmental impacts.

With the rapid development of measurement techniques, high-time-resolution measurement of OON has become more available. Currently, online measurement of OON can be conducted by the following routes: (i) by thermodenuder dissociation to  $\text{NO}_2$  and then detection by laser-induced fluorescence (TD-LIF) (Day et al., 2002; Rollins et al., 2010) or cavity-related spectroscopy (Keehan et al., 2020; Sadanaga et al., 2016); (ii) by using an aerosol mass spectrometer (AMS) (DeCarlo et al., 2006) based on  $\text{NO}_2^+/\text{NO}^+$  apportionment (Farmer et al., 2010; Fry et al., 2013; Hao et al., 2014; Day et al., 2022; Xu et al., 2015) and/or a thermodenuder (W. Xu et al., 2021); and (iii) by using a chemical ionization mass spectrometer (CIMS) with different ionization sources, typically with iodide-adduct chemistry (Huang et al., 2019; Lee et al., 2014, 2016) or extractive electrospray ionization (Bell et al., 2022; Lopez-Hilfiker et al., 2019; Pospisilova et al., 2020). Although the first two methods can quantify nitrate functional groups ( $-\text{ONO}_2$  or  $-\text{NO}_2$ ) in bulk, CIMS, by taking advantage of soft ionization, can provide information on molecular compositions and facilitate comprehension of particle-phase ONs (pONs) and nitroaromatics at the molecular level (Lee et al., 2014; Pospisilova et al., 2020; M. Wang et al., 2020; Salvador et al., 2021). In general, nitroaromatics have also been included in the quantification of ONs by the CIMS under a negative ionization mode due to the difficulty encountered in distinguishing the nitro functional group ( $-\text{NO}_2$ ) from the  $-\text{ONO}_2$  and  $-\text{NO}_2$  groups based solely on chemical formulas of ions (Huang et al., 2019). So far, gOON and pOON (containing 4–12 oxygen atoms) formed from multiple oxidation processes of volatile organic compounds (VOCs) have been quantified by a high-

resolution time-of-flight CIMS installed with the Filter Inlet for Gases and AEROSols (FIGAERO-CIMS) in forests (Lee et al., 2018, 2016) and at rural sites (Huang et al., 2019; Chen et al., 2020). However, limited measurement results were reported in the polluted urban areas (Le Breton et al., 2019).

Both primary emission and secondary formation can contribute to mass concentrations of ambient OON. Biomass burning and/or fossil fuel combustion have been suggested as important primary emission sources of gOON (Liu et al., 2017; Palm et al., 2020; Peng et al., 2021) and pOON (Gaston et al., 2016; Mohr et al., 2013; Wang et al., 2019; Zhang et al., 2016). Furthermore, secondary formation of OON in biomass burning plumes has also been observed. For example, Juncosa Calahorrano et al. (2021) observed the existence of gOON in aged plumes of wildfires. Kodros et al. (2020) showed that pOON could not only be directly emitted from laboratory-generated biomass burning emissions, but also formed quickly through nitrate radical ( $\text{NO}_3$ ) oxidation within biomass burning plumes. Based on aircraft measurements, Palm et al. (2020) found that the VOCs and vapors evaporated from primary biomass burning could be quickly subjected to radical-driven oxidation, thus contributing to the formation of SOA, including nitroaromatics. For the secondary formation pathway in ambient air, gOON is formed mainly through the oxidation of VOCs by hydroxyl radicals (OH),  $\text{NO}_3$  and ozone in the presence of  $\text{NO}_x$  (Ng et al., 2017; Perring et al., 2013). Functionalization of gOON in ambient air reduces their volatility, leading to condensation of gOON onto particles to form secondary pOON (Capouet and Müller, 2006).

Previous studies indicated that the oxidation of biogenic VOCs by  $\text{NO}_3$  dominated gOON formation at a forest–urban site in Germany (56 % of the average gOON production rate) (Sobanski et al., 2017) and at boreal forest sites in Finland (70 % of the total gOON production rate) (Liebmann et al., 2019) and the southeastern USA (84 % of the monoterpene organic nitrate mass) (Ayres et al., 2015; Pye et al., 2015; Xu et al., 2015). For urban areas, the contributions of the above-mentioned three secondary formation pathways to the total gOON remain poorly understood (Yu et al., 2019). Initiation of oxidation by OH under high- $\text{NO}_x$  conditions is traditionally regarded as the main formation pathway for urban OON during the day (Perring et al., 2013). However, Hamilton et al. (2021) recently found that a large fraction of isoprene-derived OON was formed through unexpected  $\text{NO}_3$  oxidation pathways in the afternoon in the Beijing urban area.

Thus, a better understanding of the OON sources and formation mechanisms in urban areas is still needed.

In this study, quantitative measurements of gOON and pOON were carried out using the high-resolution time-of-flight FIGAERO-CIMS and an AMS in a Chinese megacity. The contributions of biomass burning and secondary formation to ambient total gOON and pOON measured by the CIMS were quantified, and the secondary oxidation pathways were systematically explored based on the production rates of gOON. Finally, the molecular compositions of ambient OON measured by the CIMS were comprehensively investigated.

## 2 Experimental methods

### 2.1 Sampling site

Measurements were conducted on the campus of the Guangzhou Institute of Geochemistry, Chinese Academy of Sciences (23.14° N, 113.36° E), in the urban area of megacity Guangzhou during the coordinated campaign Particles, Radicals, and Intermediates from oxidation of primary Emissions over the Great Bay Area (PRIDE-GBA) (Wu et al., 2020). The observation site is located 25 m above the ground on the ninth floor of the highest building on the campus. The campus is surrounded by industrialized and urbanized downtown areas in a typically subtropical climate and is thus strongly influenced by both anthropogenic and biogenic emissions, as shown in Fig. S1. The average ambient temperature and relative humidity (RH) during the campaign were  $23.7 \pm 2.9$  °C and  $71.9 \pm 17.4$  %, respectively. The site was mostly affected by northerly winds with an average speed of  $4.5 \pm 2.18$  m s<sup>-1</sup>.

### 2.2 Measurement and analysis

#### 2.2.1 Operation of FIGAERO-CIMS

During the campaign, a CIMS installed with a long time-of-flight detector ( $10\,000 < m/\Delta m < 11\,000$ ) with an iodide source (Aerodyne Research Inc, USA) was deployed (Lee et al., 2014; Z. Wang et al., 2020). The FIGAERO inlet was installed with the CIMS to measure speciated gOON and pOON (Lopez-Hilfiker et al., 2014; Bannan et al., 2019; Schobesberger et al., 2018; Thornton et al., 2020). The detailed performance and calibration information of the CIMS can be found in a recent paper about this campaign (Ye et al., 2021). A brief description is introduced here. The sampling flow rate is  $3.8$  L min<sup>-1</sup> for the gas-sampling line and  $5$  L min<sup>-1</sup> for the particle line. A PM<sub>2.5</sub> cyclone inlet and a Nafion dryer (Perma Pure, model PD-07018T-12MSS) were set ahead of the particle-sampling inlet of the FIGAERO to keep the filter for aerosol sampling from getting wet due to the high ambient RH ( $72 \pm 17$  %) in this campaign. A recent study shows that aerosol in equilibrium with semi-volatility and intermediate-volatility organic compounds (S/IVOCs) will be perturbed by the removal of gases by the Nafion dryer

(Liu et al., 2019). However, in this study, the retention time for particles through the Nafion dryer was  $\sim 0.12$  s, which might lead to a very small change in S/IVOC signals on such a timescale (less than a few percent) based on the partitioning delay model (Pagonis et al., 2017). In addition, an accurate correction for S/IVOC loss in the Nafion dryer is not currently available (Liu et al., 2019). Thus, no S/IVOC correction of the aerosol phase was performed in this study.

In general, to measure the gOON and pOON, the FIGAERO was operated alternately at two main stages during the measurement. (i) For the first 24 min in a 1 h cycle, ambient air was continuously sampled into two inlets, i.e., gas and particle inlets. The gas inlet was connected to an ion–molecule reaction region (IMR) of the CIMS. An X-ray source was used in this campaign, which has lower ionization efficiency compared to the polonium-210 radioactive source used in the previous studies (Faxon et al., 2018; Lee et al., 2021; Palm et al., 2019). Therefore, a higher pressure (370–390 mbar) in the IMR than in previous studies (e.g., 93–200 mbar) (Faxon et al., 2018; Lee et al., 2021; Palm et al., 2019) was used to achieve similar strengths of reagent ions in the CIMS system. The sampled VOCs were first ionized in the IMR ( $\text{VOC}\cdot\text{I}^-$ ), in which the primary ions were generated by flowing  $2$  mL min<sup>-1</sup> 1000 ppm methyl iodide in  $2.4$  L min<sup>-1</sup> N<sub>2</sub> through the X-ray source and then moved into the mass spectrometer for measurement at a resolution of 1 s. Moreover, the ambient air was also introduced into the particle-sampling inlet where a sliding Teflon tray had a polytetrafluoroethylene membrane filter (Zefluor®, Pall Inc., USA) for aerosol collection for 24 min. (ii) Next, after 24 min, when the gas-phase measurement was completed, a linear actuator was used to move the Teflon tray on which the filter was placed in front of the IMR, while the gas-phase inlet was blocked. Then, ultra-high-purity N<sub>2</sub> gas at a flow rate of  $2$  L min<sup>-1</sup> was passed through a stainless-steel “heating tube” to thermally desorb the collected particles on the filter into the gas and then into the IMR and mass spectrometer for measurement. The temperature of N<sub>2</sub> flow was ramped up from room temperature to 175 °C in 12 min and then kept at 175 °C for another 20 min. The temperature of the IMR was kept almost constant by setting the temperature constant (80 °C) of the heater strip in the IMR. Meanwhile, the room temperature, which was maintained by an air conditioner, was relatively stable ( $23.7 \pm 2.9$  °C). The gas-sampling line inside the room was covered by heat insulation associated with a heating cable to hold the temperature of the sampling gas steady. These protocols reduce the effect of the temperature dependence of the IMR, as indicated by Robinson et al. (2022), that I<sup>-</sup> CIMS sensitivity may be influenced by the temperature of the IMR.

The background signal of the gas-phase measurement was determined by a pure N<sub>2</sub> signal in the last 3 min within the 24 min sampling time (Palm et al., 2019). The background signal of the particle measurement was determined by the measured signals from every sixth 1 h running cycle, in

which particle-free air was obtained with ambient air passing through a High-Efficiency Particulate Air (HEPA) filter set ahead of the FIGAERO filter (Ye et al., 2021). The ToFWare software (version 3.0.3) was used to perform high-resolution peak fitting of the CIMS mass spectra.

### 2.2.2 Oxidized organic nitrogen quantification based on CIMS measurement

Based on CIMS measurement, speciated OON (nitrogen-containing oxygenated hydrocarbons, 339 closed-shell compounds with an oxygen:carbon atom ratio of no less than 3,  $C_{\geq 1}H_{\geq 1}O_{\geq 3}N_{1-2}$ ) in both the gas and particle phases was quantified. These OON compounds can be fitted well in the high-resolution analysis after the background signals have been removed. In this study, nitroaromatics were also a subset of OON due to (i) their similar chemical and optical properties to the bulk OON compounds (He et al., 2021; Lin et al., 2017) and (ii) interferences between ONs and nitroaromatics in the CIMS measurement due to desorption and fragmentation (Ye et al., 2021). The composition of OON was mainly contributed by the CHON (one nitrogen-atom-containing species), and the  $CHON_2$  (two nitrogen-atom-containing species) only contributed 6.8 % of the gOON and 8.3 % of the pOON.

For quantification, 39 species in total, including levoglucosan ( $C_6H_{10}O_5$ ), 4-nitrophenol ( $C_6H_5NO_3$ ), 2,4-dinitrophenol ( $C_6H_4N_2O_5$ ) and 4-nitrocatechol ( $C_6H_4NO_4$ ), were calibrated with standard compounds, where the effect of humidity on the sensitivities was also accounted for (Ye et al., 2021). Their calibration factors are shown in the Excel file of the supplementary zip package of Ye et al. (2021). For other uncalibrated species, a voltage-scanning procedure was carried out every few days throughout the campaign to determine their sensitivities (including ON species) (Bi et al., 2021a, b; Lopez-Hilfiker et al., 2016). Lopez-Hilfiker et al. (2016) and Iyer et al. (2016) verified the connections between the binding energy of the iodide-adduct bond, the voltage-dissociating iodide adducts and the sensitivity of the corresponding species. The relationship between the voltage difference ( $dV$ ) and the signal fraction remaining of an iodide–molecule adduct is established by scanning the  $dV$  between the skimmer of the first quadrupole and the entrance to the second quadrupole ion guide of the mass spectrometer. This relationship curve of an individual iodide adduct can be fitted by a sigmoid function and yields two parameters:  $S_0$ , the relative signal at the weakest  $dV$  compared to the signal under the operational  $dV$ ; and  $dV_{50}$ , the voltage at which half of the maximum signal is removed (i.e., half the adducts that could be formed are declustered). A sigmoidal fit was then applied to the results of all the iodide adducts. An empirical relationship between the relative sensitivity ( $1/S_0$ ) and  $dV_{50}$  of each ion (including levoglucosan) based on average values of the entire campaign was obtained. By linking the relative sensitivity of levoglucosan

with its absolute sensitivity based on the authentic standard, the absolute sensitivity of all the uncalibrated OON species was determined after taking into account the relative transmission efficient of all the ions. The detailed data of these response factors can be found in the supporting information of Ye et al. (2021). Three OON species, which are 4-nitrophenol ( $C_6H_5NO_3$ ), 2,4-dinitrophenol ( $C_6H_4N_2O_5$ ) and 4-nitrocatechol ( $C_6H_5NO_4$ ), were calibrated with both authentic standards and voltage-scanning methods. By comparing their sensitivity (Fig. S3), the uncertainty of the voltage-scanning method can be roughly estimated. A detailed description of the calibration curves and the application of the calibration curve to estimate the sensitivity can be found in the supporting information text of Ye et al. (2021). In general, the voltage-scanning method underestimates (32 %–56 %) the sensitivity of OON in this study compared to the values using the standard compounds as real ones. This uncertainty was comparable with 30 % uncertainty of all analytes in Bi et al. (2021b) and 60 % uncertainty of total carbon in Isaacman-VanWertz et al. (2018) measured by the Iodide-CIMS. Finally, an average underestimation of 47 % on sensitivity was taken as the uncertainty of the whole OON mass loading in this study.

In summary, nitroaromatics, i.e., nitrophenol ( $C_6H_5NO_3$ ), methyl nitrophenol ( $C_7H_7NO_3$ ), dinitrophenol ( $C_6H_4N_2O_5$ ), nitrocatechol ( $C_6H_5NO_4$ ), methyl nitrocatechol ( $C_7H_7NO_4$ ) and nitrosalicylic acid ( $C_7H_5NO_5$ ), which were assumed to be identified with the ions containing the same molecule compositions detected by the CIMS (Wang et al., 2018; Wang and Li, 2021; Y. Chen et al., 2022), accounted for 18 % and 5 % of total gOON and pOON mass concentrations, respectively. Some nitroaromatic signal may be detected as elemental formulas other than those listed above, and some of the signals at the elemental formulas identified here as nitroaromatics may have contributions from ON species. While the uncertainty exists, it is likely that ONs dominated the OON observed during this campaign. For the total OON, the Iodide-CIMS may underestimate or poorly detect some types of OON, e.g., simple alkyl or keto nitrates (Lee et al., 2016). Moreover, the thermal fragmentation reactions that result from heating on the FIGAERO filter may also lead to underestimation of OON due to the loss of the nitrogen-containing groups, such as peroxy nitrates, which have the propensity to thermally dissociate into  $NO_2$  and other non-nitrogen-containing species (Lee et al., 2016).

In the ambient air, the  $C_6H_{10}O_5$  measured in the particle phase using the CIMS was probably composed of levoglucosan and its isomers (mannosan and galactosan) (Ye et al., 2021). The isomer measurement of  $C_6H_{10}O_5$  in this campaign revealed that the levoglucosan contributed  $90 \pm 2$  % mass loading of the three isomers of  $C_6H_{10}O_5$  (Jiang et al., 2023); thus, the  $C_6H_{10}O_5$  signal in this study probably can be used as a tracer for biomass burning emission (Bhattarai et al., 2019). The good correlation ( $R = 0.78$ ) between  $C_6H_{10}O_5$  and another biomass burning tracer, potas-

sium ( $K^+$ ) (Y. Wang et al., 2017; Andreae, 1983), also supports this statement (Fig. S11a). Multiple studies show that levoglucosan might be degraded due to photochemistry (Lai et al., 2014; Bai et al., 2013; Hennigan et al., 2010). We calculated the ambient photochemical age based on the ratios of two hydrocarbons (*m* + *p*-xylene and ethylbenzene) that react at different rates with OH radicals (Yuan et al., 2013; Wu et al., 2020; De Gouw et al., 2005). A daily average OH concentration of  $1.5 \times 10^6$  molec.  $\text{cm}^{-3}$  was assumed here (Mao et al., 2009; Z. Wang et al., 2020; W. Chen et al., 2021). The estimated results show that the average diurnal photochemical age varied from 0.2 d during the night to a maximum of 0.5 d in the daytime in this campaign (W. Chen et al., 2021), which was lower than the lifetime of levoglucosan (> 1 to 26 d) determined in laboratory and field studies (Hennigan et al., 2010; Hoffmann et al., 2010; Lai et al., 2014; Bai et al., 2013; Bhattarai et al., 2019). This suggests that the levoglucosan observed in this study will be stable for being the tracer of biomass burning emissions.

### 2.2.3 Other instruments

In addition to the CIMS, a high-resolution time-of-flight aerosol mass spectrometer (HR-ToF-AMS, Aerodyne Research Inc., hereafter referred to as “AMS”) was used to provide online quantitative measurement of submicron non-refractory aerosols ( $\text{PM}_{10}$ ) at a time resolution of 4 min (Canagaratna et al., 2007; DeCarlo et al., 2006). In addition to the total organic aerosol (OA), the mass concentration of the  $-\text{ONO}_2$  group from pON ( $\text{pOrgNO}_{3,\text{AMS}}$ ) was also estimated by the  $\text{NO}_2^+/\text{NO}^+$  ratio method (Farmer et al., 2010; Fry et al., 2013; Day et al., 2022; Xu et al., 2015), the positive matrix factorization (PMF) method (Hao et al., 2014) and the TD method (W. Xu et al., 2021) based on the AMS data. The  $\text{NO}_2^+/\text{NO}^+$  ratio method was based on the different ratios of  $\text{NO}_2^+$  to  $\text{NO}^+$  fragmented from  $\text{pOrgNO}_{3,\text{AMS}}$  and inorganic nitrate. The PMF method was performed by including the  $\text{NO}^+$  and  $\text{NO}_2^+$  ions in the PMF analysis combined with a spectral matrix of organic ions. The TD method was conducted based on the difference in volatility between  $\text{pOrgNO}_{3,\text{AMS}}$  and inorganic nitrates in particles. Detailed description and intercomparison of these three methods can be found in the supporting information (Sect. S1), where some insights into the pros and cons of the AMS-based methods are also presented. The comparative analysis of the CIMS and these three methods by the AMS aided in evaluating the measurement accuracy of OON in this study. Here, pON estimated by the  $\text{NO}_2^+/\text{NO}^+$  ratio method was selected as representative data for the following discussion due to the better performance achieved by this method. More detailed information on calibrations and operations of the AMS during this campaign can be found elsewhere (W. Chen et al., 2021).

VOCs were measured by online gas chromatography–mass spectrometry and using a flame-ionization detector

(GC-MS/FID) (Wuhan Tianhong Instrument Co., Ltd.) at a time resolution of 1 h and by proton-transfer reaction time-of-flight mass spectrometry (PTR-ToF-MS, IONICON Analytik) at a time resolution of 10 s (Wu et al., 2020; Yuan et al., 2017). A 56-component VOC gas standard was used for daily calibration of the GC-MS/FID (S. Wang et al., 2020). For the PTR-ToF-MS, a 16-component VOC gas standard was used for daily calibration under both dry ( $\text{RH} < 1\%$ ) and ambient humidity during the whole campaign, and an additional 23-component VOC gas standard was used during the last period of the campaign (C. Wang et al., 2020; Wu et al., 2020). The uncertainties for the VOC measurements by both instruments were below 20%. Trace gases, i.e.,  $\text{O}_3$  (TL43i),  $\text{NO}/\text{NO}_2$  (TL42i) and  $\text{CO}$  (TL48i), were measured using Thermo Fisher Scientific instruments at a time resolution of 1 min (Z. Wang et al., 2020). Meteorological parameters were measured at a Vantage Pro2 weather station (Davis Instruments) at a time resolution of 10 s.

### 2.3 Calculation of the production rates of gas-phase oxidized organic nitrogen

The production rates of gOON from VOCs oxidized by OH,  $\text{NO}_3$  and  $\text{O}_3$  were calculated using the reactant concentrations and reaction rate coefficients combined with formation-branching ratios and yields (Liebmann et al., 2019), of which the detailed calculation process can be found in Sect. S2. In this calculation, the production rates mainly from organic nitrates are shown. The parameters for secondary nitroaromatics are not available and thus are not included here. The concentrations of VOCs and  $\text{O}_3$  were obtained from direct measurements, while those of OH radicals were derived from a box model simulation with the Master Chemical Mechanism v3.3.1 (MCM v3.3.1) (S. Wang et al., 2020; Wolfe et al., 2016). The  $\text{NO}_3$  radical was calculated based on the measured  $\text{N}_2\text{O}_5$  by the CIMS (Ye et al., 2021) based on temperature equilibrium between these two species (Brown and Stutz, 2012; X. Chen et al., 2022). The remaining parameters were obtained from previous studies (Liebmann et al., 2019; Perring et al., 2013). The different VOC species and corresponding parameters are listed in Table 1. An overall uncertainty of 56% was estimated by the Monte Carlo method through 10 000 calculations in this method. The detailed uncertainties of different parameters can be found in Sect. S3.

## 3 Results and discussion

### 3.1 Quantification and chemical composition of oxidized organic nitrogen

Figure 1a shows a subset of the time series of pOON measured using the CIMS (i.e.,  $\text{pOON}_{\text{CIMS}}$ ) and  $\text{pOrgNO}_{3,\text{AMS}}$  ( $-\text{ONO}_2 + \text{NO}_2$  group) measured with the AMS. The total OA measured with the AMS is also shown in Fig. 1a. During the entire campaign, a moderate correlation (Pearson corre-

**Table 1.** The VOC species and their average mass concentrations with standard deviations. The reaction rate coefficients, branch ratios for the OH and O<sub>3</sub> pathway and yields for the NO<sub>3</sub> pathway used for the calculations of gOON production rates.

OH-initiated pathway VOC species	Average concentration (ppb)	$k_{\text{OH}}$ at 298 K (cm <sup>3</sup> molec. <sup>-1</sup> s <sup>-1</sup> )	$\alpha^{\text{RO}_2}$
Isoprene	0.15 ± 0.17	1.00 × 10 <sup>-10</sup>	0.070
<i>d</i> -Limonene <sup>a</sup>	0.07 ± 0.07	1.70 × 10 <sup>-10</sup>	0.230
$\alpha$ -Pinene <sup>a</sup>	0.07 ± 0.07	5.30 × 10 <sup>-11</sup>	0.180
Propane	6.23 ± 4.92	1.09 × 10 <sup>-12</sup>	0.036
Isobutane	1.56 ± 1.27	2.12 × 10 <sup>-12</sup>	0.096
<i>n</i> -Butane	2.80 ± 2.35	2.36 × 10 <sup>-12</sup>	0.077
Cyclopentane	0.09 ± 0.05	4.97 × 10 <sup>-12</sup>	0.045
Isopentane	1.17 ± 1.01	3.60 × 10 <sup>-12</sup>	0.070
<i>n</i> -Pentane	0.65 ± 0.65	3.80 × 10 <sup>-11</sup>	0.105
2,2-Dimethylbutane	0.03 ± 0.02	2.23 × 10 <sup>-12</sup>	0.152
2,3-Dimethylbutane	0.05 ± 0.05	2.23 × 10 <sup>-12</sup>	0.152
2-Methylpentane	0.26 ± 0.27	5.20 × 10 <sup>-12</sup>	0.097
3-Methylpentane	0.25 ± 0.25	5.20 × 10 <sup>-12</sup>	0.109
<i>n</i> -Hexane	0.50 ± 0.75	5.20 × 10 <sup>-12</sup>	0.141
2,4-Dimethylpentane	0.03 ± 0.03	3.34 × 10 <sup>-12</sup>	0.140
Methylcyclopentane	0.09 ± 0.09	5.60 × 10 <sup>-12</sup>	0.140
Cyclohexane	0.05 ± 0.05	6.97 × 10 <sup>-12</sup>	0.160
<i>n</i> -Heptane	0.09 ± 0.15	6.76 × 10 <sup>-12</sup>	0.178
Methylcyclohexane	0.07 ± 0.09	9.64 × 10 <sup>-12</sup>	0.170
<i>n</i> -Octane	0.04 ± 0.05	8.11 × 10 <sup>-12</sup>	0.226
Nonane	0.03 ± 0.03	9.70 × 10 <sup>-12</sup>	0.393
<i>n</i> -Decane	0.02 ± 0.02	1.10 × 10 <sup>-11</sup>	0.417
Benzene	0.43 ± 0.16	1.22 × 10 <sup>-12</sup>	0.034
Toluene	1.75 ± 1.86	5.96 × 10 <sup>-12</sup>	0.029
Ethylbenzene	0.28 ± 0.30	7.00 × 10 <sup>-12</sup>	0.072
<i>m-p</i> -Xylene	0.79 ± 0.82	2.30 × 10 <sup>-11</sup>	0.074
<i>o</i> -Xylene	0.29 ± 0.31	1.36 × 10 <sup>-11</sup>	0.081
Isopropylbenzene	0.01 ± 0.01	6.30 × 10 <sup>-12</sup>	0.110
<i>m</i> -Ethyltoluene	0.03 ± 0.03	1.86 × 10 <sup>-11</sup>	0.094
<i>p</i> -Ethyltoluene	0.02 ± 0.02	1.18 × 10 <sup>-11</sup>	0.137
1,3,5-Trimethylbenzene	0.02 ± 0.02	5.76 × 10 <sup>-11</sup>	0.031
<i>o</i> -Ethyltoluene	0.02 ± 0.02	1.19 × 10 <sup>-11</sup>	0.106
1,2,4-Trimethylbenzene	0.06 ± 0.06	3.25 × 10 <sup>-11</sup>	0.105
1,2,3-Trimethylbenzene	0.02 ± 0.01	3.25 × 10 <sup>-11</sup>	0.119
Propene	0.37 ± 0.37	2.63 × 10 <sup>-11</sup>	0.015
trans-2-Butene	0.03 ± 0.03	6.40 × 10 <sup>-11</sup>	0.034
1-Butene	0.07 ± 0.05	3.14 × 10 <sup>-11</sup>	0.025
cis-2-Butene	0.02 ± 0.02	5.64 × 10 <sup>-11</sup>	0.034
1-Pentene	0.03 ± 0.02	3.14 × 10 <sup>-11</sup>	0.059
trans-2-Pentene	0.01 ± 0.02	6.70 × 10 <sup>-11</sup>	0.064
cis-2-Pentene	0.01 ± 0.01	6.50 × 10 <sup>-11</sup>	0.064
1-Hexene	0.02 ± 0.01	3.70 × 10 <sup>-11</sup>	0.055
NO <sub>3</sub> -initiated pathway VOC species	Average concentration (ppb)	$k_{\text{NO}_3}$ at 298 K (cm <sup>3</sup> molec. <sup>-1</sup> s <sup>-1</sup> )	$\alpha_i$
Isoprene	0.15 ± 0.17	6.95 × 10 <sup>-13</sup>	0.700
<i>d</i> -Limonene	0.07 ± 0.07	1.22 × 10 <sup>-11</sup>	0.670
$\alpha$ -Pinene	0.07 ± 0.07	6.21 × 10 <sup>-12</sup>	0.150
Phenol	0.04 ± 0.03	3.92 × 10 <sup>-12</sup>	0.251
Cresol	0.03 ± 0.03	1.37 × 10 <sup>-11</sup>	0.128
Styrene	0.17 ± 0.26	1.50 × 10 <sup>-12</sup>	0.251 <sup>b</sup>
O <sub>3</sub> -initiated pathway VOC species	Average concentration (ppb)	$k_{\text{O}_3}$ at 298 K (cm <sup>3</sup> molec. <sup>-1</sup> s <sup>-1</sup> )	$\alpha^{\text{O}_3}$
Isoprene	0.15 ± 0.17	1.28 × 10 <sup>-17</sup>	1.000
<i>d</i> -Limonene	0.07 ± 0.07	2.20 × 10 <sup>-16</sup>	0.750
$\alpha$ -Pinene	0.07 ± 0.07	9.40 × 10 <sup>-17</sup>	0.800

Note that all the reaction rate coefficients and the formation-branching ratios or yields are from MCM v3.3.1 and previous studies (Perring et al., 2013; Liebmann et al., 2019; Atkinson and Arey, 2003). <sup>a</sup> We assumed that total monoterpenes measured from PTR-ToF-MS are composed of *d*-limonene and  $\alpha$ -pinene with a ratio of 1 : 1 based on the anthropogenic origins of monoterpene, as discussed in Sect. S2. <sup>b</sup> The parameters were assumed to be equal to that of phenol.

lation coefficient  $R = 0.42$ , Fig. S6) was observed between  $\text{pOON}_{\text{CIMS}}$  and  $\text{pOrgNO}_3_{\text{AMS}}$ , which is probably due to the high uncertainty in  $\text{pOrgNO}_3_{\text{AMS}}$  estimation from the AMS when the organic nitrate fraction in the total nitrate signal is low ( $< 10\%$ ; the details can be found in Sect. S1) and due to the fact that only the  $-\text{ONO}_2/\text{NO}_2$  groups instead of a complete ON molecule were measured with the AMS. The description of the correlation coefficient ( $R$ ) within this study is defined based on the interpretation by Dancy and Reidy (2007), as shown in detail in Sect. S1. When the mass concentration of total nitrates from the AMS is below  $5\ \mu\text{g m}^{-3}$  (corresponding to the  $\text{pOrgNO}_3_{\text{AMS}}$  signal fraction in the total nitrate signal  $> 60\%$ ), an improved correlation between  $\text{pOON}_{\text{CIMS}}$  and  $\text{pOrgNO}_3_{\text{AMS}}$  is found ( $R = 0.86$ , Fig. 1b), validating the robustness of the  $\text{pOON}_{\text{CIMS}}$  measured here. A similarly moderate correlation between  $\text{pOrgNO}_3_{\text{AMS}}$  and  $\text{pOON}_{\text{CIMS}}$  was also observed at a rural site in southwestern Germany ( $R = 0.52$ ) (Huang et al., 2019), and a much better agreement ( $R = 0.82$ ) was obtained in the southeastern USA when the  $\text{pOrgNO}_3_{\text{AMS}}$  fraction in total nitrate is above  $70\%$  (Lee et al., 2016; Xu et al., 2015).

The average concentrations of the  $\text{gOON}_{\text{CIMS}}$  and  $\text{pOON}_{\text{CIMS}}$  measured using the CIMS were  $1.00 \pm 0.67$  and  $0.66 \pm 0.53\ \mu\text{g m}^{-3}$ , respectively. Moreover, an average concentration of  $0.60 \pm 0.46\ \mu\text{g m}^{-3}$  for  $\text{pOrgNO}_3_{\text{AMS}}$  during the campaign was obtained. Notably, different size cuts between the AMS ( $\text{PM}_1$ ) and the CIMS ( $\text{PM}_{2.5}$ ) should only play a minor role in the quantification of pOON, as the measured total aerosol mass concentrations of  $\text{PM}_{2.5}$  and  $\text{PM}_1$  during the campaign are very similar (a regression slope of 0.96) (W. Chen et al., 2021). The average mass-weighted chemical compositions for  $\text{gOON}_{\text{CIMS}}$  and  $\text{pOON}_{\text{CIMS}}$  observed in this campaign were determined to be  $\text{C}_{6.6}\text{H}_{9.4}\text{N}_{1.1}\text{O}_{5.3}$  and  $\text{C}_{8.5}\text{H}_{12.2}\text{N}_{1.1}\text{O}_{6.5}$ , respectively, corresponding to molecular weights (MWs) of  $189 \pm 7.8$  and  $234 \pm 7.9\ \text{g mol}^{-1}$ . The molecular weight of  $\text{pOON}_{\text{CIMS}}$  in this study ( $234 \pm 7.9\ \text{g mol}^{-1}$ ) is comparable to the reported values at forest ( $256\ \text{g mol}^{-1}$ ) and rural ( $220$  and  $296\ \text{g mol}^{-1}$ ) sites (Lee et al., 2018; Huang et al., 2019; Chen et al., 2020). If such an average MW of  $\text{pOON}_{\text{CIMS}}$  were applied, the  $\text{pOON}_{\text{AMS}}$  (in addition to  $-\text{ONO}_2/-\text{NO}_2$  groups, the organics part was also accounted for) would be  $2.3\ \mu\text{g m}^{-3}$  based on multiplying a factor of 3.8 by  $\text{pOrgNO}_3_{\text{AMS}}$ , which is well within the range of  $0.06$ – $2.94\ \mu\text{g m}^{-3}$  of  $\text{pOON}_{\text{AMS}}$  as reported in the previous studies around the world and as shown in Fig. S7. On the other hand, if only  $-\text{ONO}_2/-\text{NO}_2$  groups are considered to calculate  $\text{pOON}_{\text{CIMS}}$  to be  $\text{pOrgNO}_3_{\text{CIMS}}$ , the calculated  $\text{pOrgNO}_3_{\text{CIMS}}$  can explain  $28 \pm 18\%$  of  $\text{pOrgNO}_3_{\text{AMS}}$ , which is consistent with the fraction ( $23\%$ ) of total functionalized OA detected using the CIMS versus total OA measured using the AMS (Ye et al., 2021). The detailed analysis process of comparison uncertainty between the AMS and the CIMS can be found in Sect. S3 of the supporting information.

For this study, an average mass fraction of  $15 \pm 12\%$  of  $\text{pON}_{\text{AMS}}$  in the total OA ( $14.7 \pm 8.20\ \mu\text{g m}^{-3}$  on average) measured by the AMS was observed (the calculation method is referred to in Takeuchi and Ng, 2019). In spite of the absolute mass concentrations of pON varying greatly in different studied urban environments, the pON/OA ratios are very similar ( $15 \pm 3\%$  on average, Fig. S7), suggesting a potentially similar pON formation process or fate in the urban areas (Day et al., 2010; Rollins et al., 2012; Xu et al., 2015).

To further illustrate the contributions of different components of speciated gOON and pOON measured by the CIMS, five  $\text{C}_x\text{N}$  groups, i.e., (1)  $\text{C}_{4-5}\text{N}$ , (2)  $\text{C}_{6-9}\text{AroN}$ , (3)  $\text{C}_{8-10}\text{N}$ , (4)  $\text{C}_{11-20}\text{N}$  and (5)  $\text{C}_{\text{others}}\text{N}$  (Fig. 1c and e), were categorized based only on the number of carbon atoms in the molecules. The  $\text{C}_{6-9}\text{AroN}$  group was recognized based on the number of six to nine carbon atoms and a positive aromaticity index (0–1) (Sect. S4) (Koch and Dittmar, 2016; Wang et al., 2019; Koch and Dittmar, 2006). The  $\text{C}_{11-20}\text{N}$  group contains species with large carbon backbones from 11 to 20 and/or oligomers, and  $\text{C}_{\text{others}}\text{N}$  includes the remaining nitrogen-containing short-chain ions which are not possible to fit into the previous four categories, such as the ions with fewer than four carbon atoms (e.g.,  $\text{C}_3\text{H}_7\text{NO}_4$  and  $\text{C}_3\text{H}_7\text{NO}_5$ ) and the ions with six to nine carbon atoms excluded in the  $\text{C}_{6-9}\text{AroN}$  group (e.g.,  $\text{C}_6\text{H}_9\text{NO}_3$  and  $\text{C}_7\text{H}_{11}\text{NO}_5$ ). In general, it is observed that the contributions of  $\text{C}_{4-5}\text{N}$  ( $25\%$ ) and  $\text{C}_{6-9}\text{AroN}$  ( $24\%$ ) to the total gOON are higher than those to the total pOON ( $14\%$  and  $16\%$ , respectively), while  $\text{C}_{8-10}\text{N}$  ( $39\%$ ) and  $\text{C}_{11-20}\text{N}$  ( $13\%$ ) contributed more to the total pOON than to the total gOON ( $26\%$  and  $4\%$ , respectively). These results are more consistent with the lower volatility for  $\text{C}_{8-10}\text{N}$  and  $\text{C}_{11-20}\text{N}$  than those for  $\text{C}_{4-5}\text{N}$  and  $\text{C}_{6-9}\text{AroN}$  due to the longer backbones of compounds in the former groups (Kroll and Seinfeld, 2008; Odum et al., 1996). In general, the time series of all groups for gOON shows similar variability to pOON (correlation coefficient  $R > 0.6$ ), except for the  $\text{C}_{4-5}\text{N}$  groups, which show a positive correlation of  $R = 0.31$  (Fig. S8). The slightly poor correlation of the  $\text{C}_{4-5}\text{N}$  groups between the gas and aerosol phases was probably caused by less partitioning of substantially formed isoprene-oxidized gOON in the daytime to pOON compared to other long-chain compounds. The regression slope between the gOON and pOON of each category (3.61 to 1.80) decreases with the increase in the carbon number, as shown in Fig. S8, which is reasonable considering their gas–particle partitioning balances (Odum et al., 1996).

The overall average diurnal variations of gOON and pOON and their  $\text{C}_x\text{N}$  groups are shown in Fig. 1d and f. Despite the boundary layer expansion in the daytime (Fig. S9a), gOON peaks in the afternoon and drops slowly, with the tail toward the night. The enhancement of gOON increases with  $j_{\text{NO}_2}$  (Fig. 1f), indicating that daytime secondary formation is an important source of gOON (Sobanski et al., 2017). The primary biomass burning (e.g., levoglucosan as

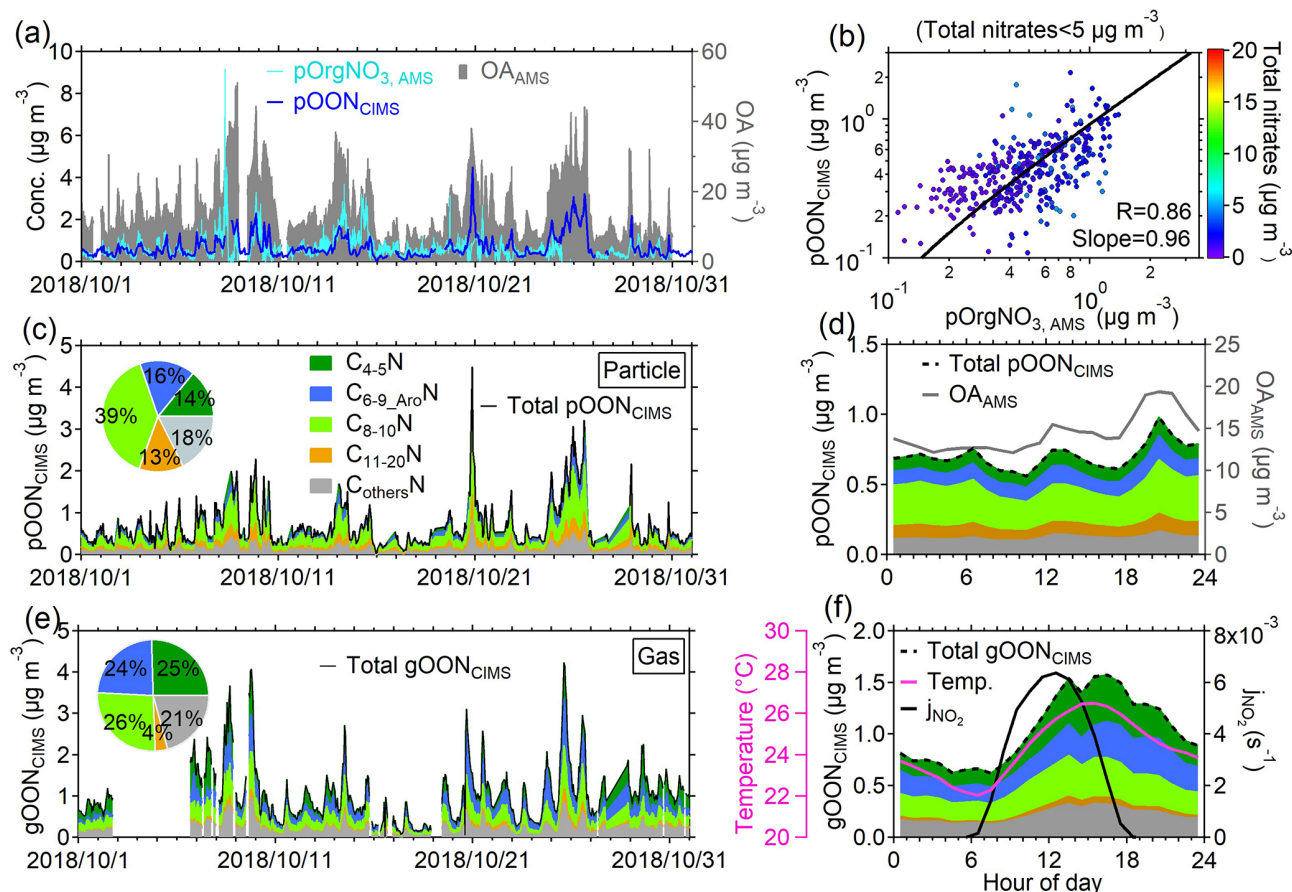


**Figure 1.** Time series and variations of OON during the PRIDE-GBA campaign. **(a)** Time series of  $\text{pOON}_{\text{CIMS}}$  and  $\text{pOrgNO}_{3,\text{AMS}}$ . The time series of the total OA detected by the AMS is shown on the right axis. **(b)** Scatterplot of  $\text{pOON}_{\text{CIMS}}$  versus  $\text{pOrgNO}_{3,\text{AMS}}$  during the campaign. The term “total nitrates  $< 5 \mu\text{g m}^{-3}$ ” indicates that the data used in this scatterplot are under the condition that the mass concentration of total nitrates (including organic nitrate and inorganic nitrate) measured by the AMS is lower than  $5 \mu\text{g m}^{-3}$ . The points are color-coded using the total nitrate signals measured by the AMS. The scatterplot from all AMS and CIMS measurements can be found in Fig. S6. The logarithm was applied to both of the axes. Time series of **(c)**  $\text{pOON}_{\text{CIMS}}$  and **(e)**  $\text{gOON}_{\text{CIMS}}$  as well as the time series of their  $\text{C}_x\text{N}$  groups from the CIMS measurement. The insets show their average mass contributions to total  $\text{gOON}_{\text{CIMS}}$  and  $\text{pOON}_{\text{CIMS}}$  during the campaign, respectively. The average diurnal variations of **(d)**  $\text{pOON}_{\text{CIMS}}$ , its  $\text{C}_x\text{N}$  groups and OA. **(f)** Average diurnal variations of total  $\text{gOON}_{\text{CIMS}}$ , its  $\text{C}_x\text{N}$  groups, the photolysis rate of  $\text{NO}_2$  ( $j_{\text{NO}_2}$ ) and temperature during the entire campaign. All the diurnal variations calculated throughout the paper are based on the average values. All the linear fittings are based on the orthogonal distance regression (ODR) algorithm in this study. All the abbreviations can be found in Appendix A.

a tracer) and vehicle emissions (e.g.,  $\text{NO}/\text{NO}_x$  as tracers), which are also potential sources of  $\text{gOON}$ , visually show enhancement during nighttime (levoglucosan and isomers in Fig. S11f and  $\text{NO}/\text{NO}_x$  in Fig. S9b) and morning rush-hour time ( $\text{NO}/\text{NO}_x$  only), respectively, in their diurnal variations, indicating that both primary sources are unlikely to contribute to the  $\text{gOON}$  enhancement during daytime. In contrast to  $\text{gOON}$ ,  $\text{pOON}$  exhibits two peaks during the afternoon and nighttime (Fig. 1d), indicating the possibility of different sources and formation mechanisms for  $\text{pOON}$  compared to  $\text{gOON}$ , e.g., biomass burning contribution during nighttime (Rollins et al., 2012). A more detailed analysis of

the sources of  $\text{gOON}$  and  $\text{pOON}$  is presented in the next section.

In general, the average diurnal concentration of each  $\text{gOON}$  ( $\text{pOON}$ ) group shows a similar trend (Fig. S9d and g). The fraction of the  $\text{C}_{4-5}\text{N}$  group in  $\text{gOON}$  enhances slightly during daytime (Fig. S9e), which might be due to strong photochemical formation of isoprene nitrates (Fisher et al., 2016; Reeves et al., 2021; Mayhew et al., 2022; Hamilton et al., 2021). The  $\text{C}_{8-10}\text{N}$  fraction in total  $\text{pOON}$  slightly enhances during nighttime (Fig. S9h), which was probably due to the primary emissions and the formation of monoterpene nitrates by  $\text{NO}_3$  oxidation chemistry (Peng et al., 2021; Fisher et al., 2016).

### 3.2 Source apportionment of oxidized organic nitrogen

To elucidate the sources of OON measured using the CIMS, the correlations between OON and a wide range of trace species representing different sources were explored to filter the best tracer for source apportionment. The scatterplots of gOON and pOON (hereafter represented by gOON<sub>CIMS</sub> and pOON<sub>CIMS</sub>) with selected species, including particle-phase C<sub>6</sub>H<sub>10</sub>O<sub>5</sub> (levoglucosan and its isomers), were created using the CIMS; *m/z* 60 measured using the AMS, benzene, NO<sub>x</sub> and CO is shown in Figs. 2 and S10. It was observed here that the scatterplots of gOON (and pOON) versus C<sub>6</sub>H<sub>10</sub>O<sub>5</sub>, the tracer for biomass burning emissions (Y. Li et al., 2021; Simoneit, 2002; Simoneit et al., 1999), exhibit two different regression slopes during daytime and nighttime (Fig. 2a and c). However, different regression slopes were not observed in the scatterplots of OON versus other tracers, e.g., CO or benzene. This suggests that the biomass burning which usually peaks during the night might be an important source of OON. The time series of OON, in particular pOON, indeed peak consistently with C<sub>6</sub>H<sub>10</sub>O<sub>5</sub> during high-concentration episodes (Figs. S12a and S13a), indicating that biomass burning emissions contributed substantially to OON during this campaign. Other biomass burning tracers, e.g., *m/z* 60, did not show a separated regression slope with OON, which is probably due to the elevated background of *m/z* 60 contributed by non-biomass burning emissions (Cubison et al., 2011; Mohr et al., 2009). Another two potential biomass burning tracers, i.e., C<sub>7</sub>H<sub>8</sub>O<sub>2</sub> (methoxyphenol and its isomers) and C<sub>8</sub>H<sub>8</sub>O<sub>4</sub> (vanillic acid and its isomers), the former exhibiting a relatively low concentration and the latter showing a larger background than C<sub>6</sub>H<sub>10</sub>O<sub>5</sub> (levoglucosan and its isomer) (Fig. S11), are both not the ideal biomass burning tracers in this study.

In contrast to those C<sub>6</sub>H<sub>10</sub>O<sub>5</sub> and OON peaks consistent with each other, the time series of OON did not peak during the episodes with strong influences of vehicle emissions (as indicative of high NO and NO<sub>x</sub> concentrations > 50 ppb) (Harrison et al., 2003; Wormhoudt et al., 2015), as shown in Figs. S14a and S15a. In addition, anticorrelations between OON and NO/NO<sub>x</sub> during some of these episodes were even found, indicating that vehicle emission is not a significant source of primary OON. Furthermore, it was found that the diurnal variation in pOON peaks 1 h earlier than NO<sub>x</sub> in the morning, thus supporting their different origins (Fig. S15g). The coincidence of the peaking time between pOON and NO<sub>x</sub> during nighttime is probably more influenced by biomass burning. Another piece of evidence is that multiple laboratory studies found negligible emissions of gOON from emission tests of vehicle exhaust based on Iodide-CIMS direct measurement (Le Breton et al., 2019; T. Li et al., 2021). Thus, the biomass burning emissions and secondary formation should be the main sources of OON observed in this campaign.

To quantify the contributions of biomass burning (OON<sub>bb</sub>) and secondary formation (OON<sub>sec</sub>) to OON in both the gas and particle phases, the following Eqs. (1) and (2) were proposed to allocate the OON sources:

$$\text{OON}_{\text{bb}} = ([\text{OON}_{\text{measured}}]/[\text{levo.}])_{\text{bb}} \times [\text{levo.}], \quad (1)$$

$$\text{OON}_{\text{sec}} = \text{OON}_{\text{measured}} - \text{OON}_{\text{bb}}, \quad (2)$$

where [levo.] is the concentration of particulate C<sub>6</sub>H<sub>10</sub>O<sub>5</sub> measured using the CIMS, and ([OON<sub>measured</sub>]/[levo.])<sub>bb</sub> is the averaged ambient concentration ratio determined from slopes between ambient OON and particulate C<sub>6</sub>H<sub>10</sub>O<sub>5</sub> during selected episodes with strong influences of biomass burning (Figs. S12 and S13). This approach relies on a concept similar to the widely used “elemental carbon tracer method” for source apportionment of primary and secondary organic carbon (Turpin and Huntzicker, 1995). A similar method was used by Salvador et al. (2021) to quantify the sources of nitroaromatic compounds. The episodes were selected based on the following three criteria. (1) The peak concentration of C<sub>6</sub>H<sub>10</sub>O<sub>5</sub> should be above 0.2 μg m<sup>-3</sup> for selecting periods strongly influenced by biomass burning plumes. (2) The regression coefficient *R* between gOON (pOON) and C<sub>6</sub>H<sub>10</sub>O<sub>5</sub> during each episode should be > 0.7. (3) The number of fitting points during each episode should be above 4 due to the hourly data of particle-phase C<sub>6</sub>H<sub>10</sub>O<sub>5</sub> being used. The averaged ambient concentration ratios were determined to be 3.95 ± 1.67 μg m<sup>-3</sup>/μg m<sup>-3</sup> for gOON and 5.05 ± 1.01 μg m<sup>-3</sup>/μg m<sup>-3</sup> for pOON, as presented in Table S1. The variability of [OON<sub>measured</sub>]/[levo.] ratios from multiple biomass burning episodes for pOON is 20 %. The slightly larger ratio uncertainty for gOON (42 %) is mainly due to active gas-phase reaction and low contributions of biomass burning emissions to the total gOON, as discussed below.

The ratios, i.e., ([OON<sub>measured</sub>]/[levo.])<sub>bb</sub>, were obtained based on ambient measurement; therefore, the ratios might be influenced by secondary formation within biomass burning plumes, and the OON<sub>bb</sub> here is referred to as the total primary and rapidly formed secondary OON from biomass burning emissions. OON<sub>sec</sub> is defined as secondary OON from non-biomass burning sources, e.g., biogenic and non-biomass burning anthropogenic sources and possible OON slowly formed from biomass burning sources (i.e., the next day), which will be minor. By using this approach, the estimated diurnal variation and time series of OON<sub>bb</sub> and OON<sub>sec</sub> are shown in Figs. 2 and 3. Compared with the measured total OON, the OON<sub>sec</sub> exhibits better agreement with the total gOON production rate in terms of both time series and correlation coefficients (*R* increases from 0.61 to 0.65 for gOON and from 0.19 to 0.45 for pOON: Fig. S16). In particular, better agreement was found from 24 to 26 October 2018, when the contribution of biomass burning to OON was high. The precursors, e.g., alkanes, alkenes, aromatics (phenol and cresol) and terpenes (isoprene and monoter-

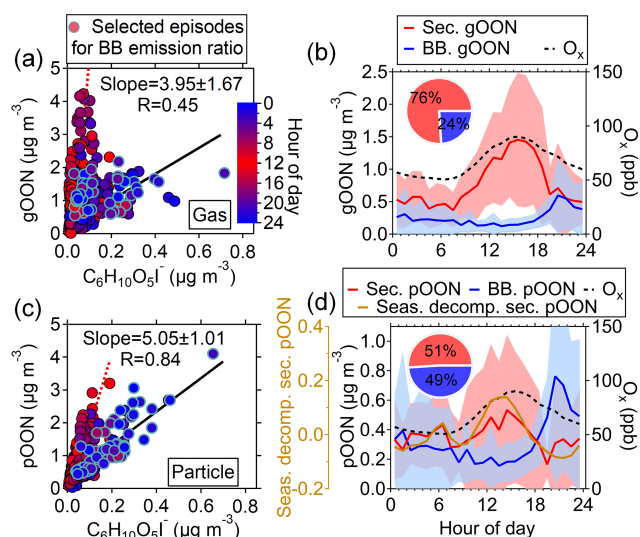


**Figure 2.** Scatterplots of (a) gOON and (c) pOON versus  $C_6H_{10}O_5I$  measured by the CIMS with the data points color-coded using the hour of the day. The blue circles indicate the data points from multiple strongly influenced episodes by biomass burning emission, of which the ratios between gOON or pOON and  $C_6H_{10}O_5I$  were used to determine the average ratio (black regression line). The red dotted line means the line regression during the daytime. The diurnal variations of (b) gOON and (d) pOON are from biomass burning (BB) and secondary formation (sec.). The shaded areas mean the standard deviations. The seasonal decomposed secondary pOON (the corresponding method is referred to in Sect. S4) and  $O_x$  are also shown. The inset pies are the contributions from biomass burning and secondary formation to total gOON and pOON, respectively.

penes), considered in the calculation were also contributed by biomass burning (Liu et al., 2017; Gilman et al., 2015), especially during the strong biomass burning emission period. The particle-phase  $OON_{sec}$  also showed consistent variation ( $R = 0.70$ ) with semi-volatile oxygenated OA (SV-OOA), which was treated as freshly formed SOA during the day (Fig. S17) (W. Chen et al., 2021), supporting the secondary origins of  $pOON_{sec}$ . These results validated the source apportionment of OON applied here.

On average, biomass burning emissions accounted for  $49 \pm 23\%$  of the total pOON measured by the CIMS, while the contribution was much lower ( $24 \pm 25\%$ ) for gOON (Fig. 2b and d), indicating that biomass burning is one of the major sources of pOON measured by the CIMS and that gOON is predominately from secondary formation ( $76 \pm 25\%$ ) (Huang et al., 2019; Lee et al., 2016). The uncertainty of these ratios represents the error of this source apportionment method, the detailed calculation process of which can be found in Sect. S3 of the supporting information. The high contribution of biomass burning to the total pOON is also consistent with the results of relevant previous studies (Mohr et al., 2013; Wang and Li, 2021; Y. Wang et al., 2017, 2019), in which substantial OON compounds were ob-

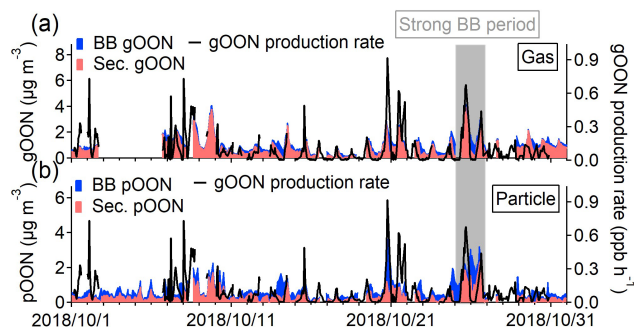


**Figure 3.** Stacked time series of secondary and biomass burning (a) gOON and (b) pOON. The gOON production rate is presented on the right axis in both of the figures. The grey period represents a strong biomass burning emission period during 24–26 October 2018, which was selected based on the high mass concentrations of  $C_6H_{10}O_5I$  and other biomass burning tracers in their time series in Fig. S11.

served in biomass burning plumes. In this study, the nighttime enhancement of  $C_6H_{10}O_5I$  indicates that the influence of biomass burning at this site was mainly contributed by the plumes of the agricultural residue combustion transported from the vicinity of Guangzhou, as shown in the MODIS wildfire point plot in Fig. S18 (L. Wang et al., 2017; Yuan et al., 2010). Moreover, the ambient ratio of  $C_6H_{10}O_5I$  to water-soluble potassium ( $K^+$ ) ( $0.20 \pm 0.04$ ) observed in this study also supports the finding that the biomass burning at this site was contributed by the combustion of crop residuals (0.1–0.2) rather than wood combustion (5.8–24.0) (Cheng et al., 2013). Figure S19 presents the Van Krevelen diagram of all OON compounds in this study. The appearance of OON compounds observed here is linked to both fresh and aged biomass burning emissions (Wang et al., 2019). In general, most of the biomass burning OON was found in the particle phase, indicating that the OON formed in biomass burning plumes has a generally lower volatility than OON formed via  $O_3$ ,  $NO_3$  oxidation or OON oxidized from non-biomass-burning-related precursors.

Based on the diurnal pattern, secondary gOON peaks form during the afternoon ( $1.49 \pm 0.49 \mu g m^{-3}$ ), which is consistent with the peaking time of  $O_x$  ( $[O_x] = [O_3] + [NO_2]$ ), and then reduce rapidly to  $0.43\text{--}0.83 \mu g m^{-3}$  at night (Fig. 2b). The similarly averaged diurnal variations of gOON and  $O_x$  indicate that the daytime chemistry corresponds to the major formation pathway of gOON. Secondary pOON also shows a slight peak ( $0.39 \pm 0.07 \mu g m^{-3}$ ) corresponding to  $O_x$  during daytime but exhibits much larger uncertainty than the secondary gOON. To elucidate this large uncertainty, a seasonal decomposition method (Hilas et al., 2006), which was performed by locally weighted linear regression to decompose the time series into three components, i.e., trend component, seasonal component and remainder, was applied (the detailed process can be found in Sect. S4). By replacing seasonal vari-

ation with hourly variation, the method can down-weight the impact of daily peak intensity variation. A clear diurnal variation of secondary pOON after seasonal decomposition is displayed in Fig. 2d, which supports the daytime peak of secondary pOON. During nighttime, the concentration of pOON ( $0.32 \pm 0.07 \mu\text{g m}^{-3}$ ) remains at a high level with a peak at 06:00 (Fig. 2d), indicating that there is a different formation pathway or formation yield for secondary pOON compared to secondary gOON at night. It is speculated that the enhanced secondary pOON formation at night is probably associated with a higher yield of pOON from  $\text{NO}_3$  chemistry and heterogeneous reactions of  $\text{NO}_3$  and  $\text{N}_2\text{O}_5$  at the particle surface, which is discussed in detail in the following section. Following Eqs. (1) and (2), the averaged concentration ratios for each category of particle-phase  $\text{C}_x\text{N}$  ( $\text{pC}_x\text{N}$ ) were also calculated separately; thus, the contributions of biomass burning and secondary formation for each  $\text{pC}_x\text{N}$  group were estimated (Fig. S20). The contribution from biomass burning to each  $\text{pC}_x\text{N}$  group only shows a small difference, ranging from 52 % for the  $\text{C}_{6-9\text{Aro}}\text{N}$  group to 40 % for the  $\text{C}_{4-5\text{N}}$  group, indicating that biomass burning is an important source of OON at wide carbon numbers.

### 3.3 Secondary formation pathways of oxidized organic nitrogen

To further elucidate the secondary formation mechanism of gOON, the diurnal patterns of gOON production rates from the three pathways following the procedure mentioned in Sect. 2.3 are calculated and shown in Figs. 4a and S21. Although the production rate did not consider the loss of OON, the calculation of the production rate still serves as a useful tool for assessing the formation pathway and precursor contribution to OON (Liebmann et al., 2019; Sobanski et al., 2017; Hamilton et al., 2021). As expected, the gOON production rates from OH- and  $\text{O}_3$ -initiated oxidation ( $0.14$  and  $0.01 \text{ ppb h}^{-1}$ , respectively) peaking at noon (11:00–13:00) are due to the high concentrations of these two oxidants during this period ( $3.9 \times 10^6$  and  $1.4 \times 10^8 \text{ molec. cm}^{-3}$ , respectively) (S. Wang et al., 2020). Interestingly, the gOON production rate from  $\text{NO}_3$ -initiated oxidation peaks at around  $0.10 \pm 0.18 \text{ ppb h}^{-1}$  from late afternoon to evening (16:00–19:00, Fig. 4a). This is mainly due to the high- $\text{NO}_3$  concentration ( $2.08 \pm 1.32 \text{ ppt}$ , Fig. S4d) when the low  $\text{NO}$  ( $1.37 \pm 0.34 \text{ ppb}$ ), moderate  $\text{O}_3$  ( $53 \pm 34 \text{ ppb}$ ) and moderate  $\text{NO}_2$  ( $31 \pm 13 \text{ ppb}$ ) (Fig. S9b) concentrations appear during that time of the day. The precursors, i.e., cresol, phenol, isoprene and monoterpenes, do not show rising concentrations during the period (16:00–19:00) except for some aromatics (Fig. S9c, f and i), indicating that not the precursor VOC but the high  $\text{NO}_3$  concentration is the main contributor to this enhancement of the  $\text{NO}_3$ -initiated gOON production rate during the day. The inconsistent peaks for the secondary gOON production rate and the secondary gOON mass loading may be due to the (i) counteraction of photochemical formation

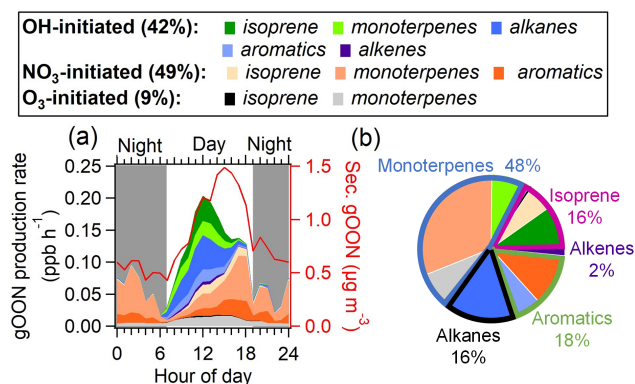


**Figure 4.** (a) Average diurnal variations of categorized gOON production rates and the concentration of secondary gOON for the whole campaign. (b) Contributions of various VOC precursors to the total gOON production rate.

and degradation and/or the (ii) effect of survivor bias from measured VOCs (Z. Wang et al., 2022; Perring et al., 2013).

In general, OH- and  $\text{NO}_3$ -initiated oxidation pathways dominated the secondary gOON formation in this study and accounted for 42 % and 49 %, respectively, of the total gOON production rate, while the rest was attributed to the  $\text{O}_3$ -initiated oxidation pathway (9 %). Figure S21 shows that the contribution to the total gOON production rate from 08:00 to 14:00 mainly came from OH chemistry (73 %) and then quickly changed to  $\text{NO}_3$  chemistry during the late afternoon (mean 55 %) and onward (mean 86 % at night). These results emphasize the importance of  $\text{NO}_3$  chemistry for the gOON production rate later in the day and the entire night in this urban area. The importance of  $\text{NO}_3$  chemistry for OON formation was also found in other locations. For example, high contributions of  $\text{NO}_3$  chemistry to the secondary gOON production rate in the Finnish boreal forest (41 % during the day and almost 100 % at night) (Liebmann et al., 2019) and the isoprene-derived gOON production rate in the Beijing urban area (32 % in the afternoon and 86 % at nighttime) (Hamilton et al., 2021) were observed. The low contribution of the  $\text{O}_3$  pathway (9 %) at this site is also consistent with the estimated fraction (12 %) in the forest area (Liebmann et al., 2019).

Figure 4b displays the contributions to the gOON production rate from different VOC precursors, among which monoterpenes account for 48 % of the total gOON production rate. The remaining contribution is attributed to biogenic VOCs, i.e., isoprene (16 %) and other anthropogenic VOCs, including aromatics (18 %), alkanes (16 %) and alkenes (2 %). These results indicate that monoterpenes are the largest contributor to the secondary formation of multifunctional gOON in this urban region. Relatively high concentrations of monoterpenes were observed during the campaign (mean:  $0.14 \pm 0.14 \text{ ppb}$ ; range: 0.003–1.5 ppb). Strong correlations of the daily averaged values from nighttime monoter-

penes with two tracers of volatile chemical product (VCP) sources (C8 aromatics,  $R = 0.85$ ; ethanol,  $R = 0.78$ ) and moderate correlations with CO ( $R = 0.62$ ) and the biomass burning tracer  $C_6H_{10}O_5$  ( $R = 0.50$ ) (Fig. 5) were also found. These strong and moderate correlations with monoterpene are in contrast to the poor correlations of these anthropogenic tracers with biogenic-derived isoprene during daytime ( $R = -0.09$  to  $0.20$ , Fig. S22). The ambient ratio of monoterpenes to CO ( $1.82 \text{ ppb ppm}^{-1}$ ) determined in Fig. 5c is significantly higher than their emission ratios from vehicle exhausts ( $0.001\text{--}0.35 \text{ ppb ppm}^{-1}$ ) (S. H. Wang et al., 2022). Combining these results, it was concluded that the monoterpenes observed during this campaign should be mainly of anthropogenic origin (Hellén et al., 2012), with VCPs as the potentially most important source. Recent studies in the USA also demonstrated that monoterpenes are strongly emitted by the VCP sources in highly populated areas (Coggon et al., 2021; Gkatzelis et al., 2021). In addition, a field study conducted in the tower located in the Guangzhou urban area found the ambient monoterpenes at an altitude of 450 m to predominantly come from VCP sources (Li et al., 2022), which is consistent with the findings here. In summary, considering monoterpenes of anthropogenic origin, anthropogenic VOCs accounted for 80 % of the total gOON production rate. Note that certain contributions of biogenic-derived monoterpenes might offset the anthropogenic-origin OON; however, other anthropogenic VOCs, such as long-chain or cyclic alkanes and/or alkenes (C. Wang et al., 2020; Zhao et al., 2016), which are important precursors for OON in urban areas (Lee et al., 2015; Lim and Ziemann, 2009; Matsunaga and Ziemann, 2010), were not considered here due to the omission of data. Thus, the anthropogenic contribution to the gOON estimated via secondary gOON production rates might still be biased low.

Figure 6a shows a strong correlation between secondary gOON and  $O_x$  ( $R = 0.83$ , slope =  $0.02 \mu\text{g m}^{-3} \text{ ppb}^{-1}$ ), which is expected as the major channel of gOON formation between peroxy radicals ( $RO_2$ ) and NO can lead to the formation of OON and  $O_3$  by continual radical propagation and photolysis of  $NO_2$  (Perring et al., 2013; L. Xu et al., 2021). Figure 6b demonstrates that secondary pOON shows a moderate correlation ( $R = 0.39$ ) with  $O_x$  and that the secondary pOON/ $O_x$  ratio increases as a function of RH (from  $\sim 0.002$  to  $\sim 0.03 \mu\text{g m}^{-3} \text{ ppb}^{-1}$ ), aerosol liquid water content (ALWC) (Fig. S23b) and wet aerosol surface area (Fig. S23c). The elevated RH and ALWC may lead to an increase in the aerosol surface area to facilitate more highly functionalized and water-soluble gOON partitioning into the particle phase and/or to promote  $NO_2$ ,  $NO_3$  and/or  $N_2O_5$  uptake into the aerosol phase (George et al., 2015; George and Abbatt, 2010). Moreover, aerosols become more liquified at higher RH, thus leading to an increase in molecular diffusion in aerosols to promote heterogeneous reactions (George et al., 2015) of  $NO_3$  with unsaturated species (Xiao and Bertram, 2011; Zhao et al., 2011),  $NO_2$  with aromatic species

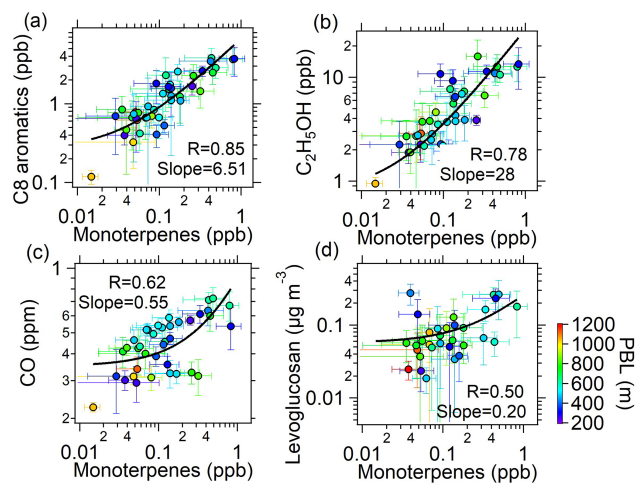


**Figure 5.** Scatterplots between the averaged concentrations of (a) C8 aromatics, (b) ethanol, (c) CO and (d)  $C_6H_{10}O_5$  versus monoterpenes at night (19:00–06:00 the next day) during the entire campaign. The color represents the planetary boundary layer height (PBL). The error bars are the standard deviations of average values during nighttime. The logarithm was applied to both of the axes.

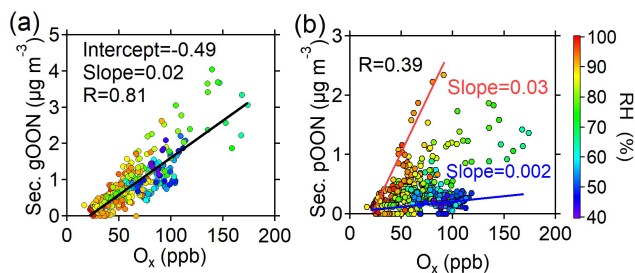


**Figure 6.** Scatterplots of (a) secondary gOON and (b) secondary pOON versus  $O_x$  color-coded using RH during the campaign. The red and blue lines are plotted to guide the eye.

and  $N_2O_5$  with alcohols to form pOON (Gross et al., 2009; Lee et al., 2015). Indeed, a lower gas–particle partitioning coefficient (saturation mass concentration,  $C^*$ ) of OON at  $RH > 70\%$  than at low  $RH (< 70\%)$  was found (Fig. S24a), which supports the favored pOON formation from heterogeneous reactions. A study in an anthropogenic-emission-dominated region also showed that the heterogeneous reactions through  $N_2O_5$  uptake can explain around half of the formation of particle-phase alkyl nitrates (Lee et al., 2015), thus signifying the important contribution of heterogeneous reactions to pOON. The secondary pOON/ $O_x$  ratio shows a much worse correlation with temperature (Fig. S23d), indicating that the lower temperature-induced higher partitioning to particles contributes little to higher pOON during nighttime.

Furthermore, the lifetime of gOON in this study can be approximately estimated by a steady-state approach (gOON mixing ratio versus total production rate) as shown in Lieb-

mann et al. (2019). A scatterplot of the secondary gOON versus the secondary gOON production rate at 1 h time resolution is shown in Fig. S24b. The roughly estimated lifetime of the secondary gOON is around 0.54–0.78 h during daytime and nighttime, respectively, which is shorter than the lifetime of alkyl nitrates ( $\sim 2 \pm 3$  h) found in boreal forest (Liebmann et al., 2019). This might be associated with the stronger photolysis, oxidative degradation and different chemical compositions of gOON in urban areas compared to boreal forest (Perring et al., 2013). The incomplete measurement of gOON by the CIMS was one of the potential reasons as well. For the lifetime of pOON, a modeling study including an explicit formation mechanism as conducted by Lee et al. (2016) is required for systematic explorations in the future.

### 3.4 Molecular chemical compositions of oxidized organic nitrogen

In this section, the molecular components of the gOON and pOON measured by the CIMS categorized with different oxygen and carbon atom numbers are briefly discussed. Figure 7 shows an overview of the distribution of molecular OON during the entire campaign, gOON during the secondary-dominated period and pOON during the BB-dominated period. In general, the gOON abundance is dominated by C<sub>5</sub>–C<sub>8</sub> and C<sub>10</sub> compounds (65 %–70 %), while pOON shows peaks around C<sub>8</sub> and C<sub>10</sub> compounds. The highly oxidized molecules (containing at least six oxygen atoms) contributed 44 % and 71 % to gOON and pOON, respectively. By comparing the ion distribution of total gOON in the whole campaign versus in the period dominated by secondary sources (Fig. 7a), we found that the mass concentration fraction of C<sub>4</sub> compounds in total gOON is much enhanced, while C<sub>6</sub> and C<sub>10</sub> compounds are significantly decreased. The enhanced C<sub>4</sub> compounds (e.g., C<sub>4</sub>H<sub>7</sub>NO<sub>5</sub> as the most-abundant ion in gOON, Fig. S19) are probably contributed by the isoprene oxidation during the day (Wennberg et al., 2018; Brownwood et al., 2021). The decreases in C<sub>6</sub> and C<sub>10</sub> compounds in gOON during the secondary-dominated period indicate that a large fraction of these compounds might come from biomass burning sources. For example, C<sub>6</sub>H<sub>5</sub>NO<sub>3</sub> (nitrophenol and its isomers) in C<sub>6</sub> is the second-most-abundant (7.4 %) compound in gOON. Multiple ambient studies have shown that biomass burning emissions can contribute substantially to C<sub>6</sub>H<sub>5</sub>NO<sub>3</sub> (Mohr et al., 2013; Wang et al., 2018), e.g., 58 % in Beijing (Song et al., 2021), consistent with the findings shown here.

The almost identical distributions of pOON during the whole campaign and the BB-dominated period mainly result from approximate contributions from biomass burning (49 % and  $\sim 70$  %, respectively). The C<sub>10</sub> compound contributions are high in both pOON ( $\sim 22$  %) during the whole campaign and the BB-dominated period (biomass burning contribution of pOON > 60 %, Fig. S25b), confirming the important contribution of biomass burning to these types of compounds

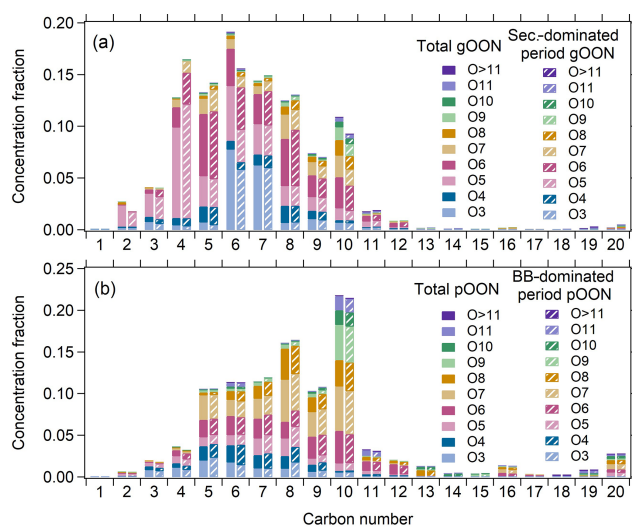


**Figure 7.** Concentration fractions of (a) gOON categorized based on carbon numbers and oxygen numbers during the whole campaign and the secondary formation-dominated period (13:00–15:00) (Fig. S25a). A similar plot is displayed for (b) pOON during the whole campaign and the BB-dominated period (19:00–21:00) (Fig. S25b).

(Fig. 7b). In pOON, the abundance of C<sub>10</sub>H<sub>x</sub>NO<sub>y</sub> ( $y \geq 6$ ) in pOON (19 %) is higher than that in gOON (9 %), which is reasonable due to their low volatility with multiple functional groups (Odum et al., 1996). The extremely oxidized C<sub>10</sub> compounds (containing at least eight oxygen atoms) might come from multiple oxidation steps and autoxidation mechanisms (Iyer et al., 2021; Zhao et al., 2018; Pye et al., 2019; Shen et al., 2021; Mayorga et al., 2022), demonstrating that the complex secondary formation processes indeed happened within the biomass burning plumes. There are high mass peaks at the positions corresponding to C<sub>16</sub> and C<sub>20</sub> species in pOON (Fig. 7b), which are oligomers. These ions might come from direct emission and/or oxidation processes in biomass burning plumes, e.g., dimerization of C<sub>8</sub> and C<sub>10</sub> species (Wu et al., 2021; Lee et al., 2018).

## 4 Conclusions

The mass concentrations, sources and formation mechanisms of gas-phase and particle-phase OON were systematically investigated in a megacity in southern China. The good comparison of pOON measured by the AMS and iodide-adduct FIGAERO-I-CIMS indicates that the CIMS can measure a fraction of  $28 \pm 18$  % of the total pOON in this study. Compared to the AMS, the missed pOON mass measured by the CIMS is probably due to the lack of detection of less-polar OON (keto and alkyl ONs) and/or non-nitrogen-containing pOON resulting from the loss of the  $-\text{NO}_2$  group by thermal desorption in CIMS measurement.

Using  $C_6H_{10}O_5$  ( $\sim 90\%$  of levoglucosan) as the biomass burning tracer for source apportionment, almost half of the pOON measured by the CIMS is attributed to biomass burning in this study, underscoring the important contribution of biomass burning to pOON in this urban area. Biomass burning is a very common source across the world. The proposed estimation method in this study might help to clarify the exact biomass burning contribution to OON and its potential atmospheric implication. Note that the sources of the undetected pOON from the CIMS are still unknown, which will be investigated further. The gOON measured by the CIMS was mainly produced by secondary formation processes (76%) initiated by OH (42%) and  $NO_3$  (49%) chemistry. The significant contribution of  $NO_3$  chemistry to gOON and potentially to other secondary products, e.g., SOA, was observed not only in Guangzhou, but also in the megacity of Beijing (Hamilton et al., 2021), highlighting the important daytime  $NO_3$  chemistry in urban areas. This indicates that the importance of daytime  $NO_3$  chemistry might not be unique and should be considered in other locations that are impacted by strong anthropogenic emissions. By ranking the precursors of OON in the ambient atmosphere, monoterpenes are determined to be the most important VOC precursors for secondary gOON formation. Much evidence suggests that the monoterpene observed in this study has anthropogenic origins from the VCP source. The monoterpene isomer measurement, which has seldom been carried out in current Chinese urban areas, is highly recommended for future studies to evaluate the impact of biogenic and anthropogenic emissions (e.g., VCPs) on ozone and other secondary products in the ambient atmosphere.

Furthermore, in this study, it is also found that heterogeneous reactions might contribute substantially to the secondary formation of pOON in urban areas; however, the detailed mechanism and its quantified contribution to pOON in ambient air are still unclear, which warrants further investigation. A thorough comparison between simulative and measured pOON might shed light on this question. Highly functionalized gOON and pOON as well as oligomers can be formed through multigenerational oxidation and autoxidation during biomass burning plumes, highlighting the complexity of sources and chemical processes in the urban environment. The results of this study provide valuable data and insights to understand the chemistry of reactive organic nitrogen in urban areas.

## Appendix A: Summary of the abbreviations

**Table A1.** The summary of the abbreviations and their corresponding full names in this study.

Abbreviation	Full name	Abbreviation	Full name
ALWC	Aerosol liquid water content	ONs	Organic nitrates
C <sub>11–20</sub> N	Oxidized organic nitrogen molecules with 11–20 carbon atoms	OON	Oxidized organic nitrogen
C <sub>4–5</sub> N	Oxidized organic nitrogen molecules with four to five carbon atoms	OON <sub>bb</sub>	Oxidized organic nitrogen from biomass burning
C <sub>6–9Aro</sub> N	Oxidized organic nitrogen molecules with six to nine carbon atoms and benzene rings	OON <sub>sec</sub>	Oxidized organic nitrogen from secondary formation
C <sub>8–10</sub> N	Oxidized organic nitrogen molecules with 8–10 carbon atoms	O <sub>x</sub>	Odd oxygen, sum of O <sub>3</sub> and NO <sub>2</sub>
CHON	Oxidized organic nitrogen with only one nitrogen atom	pC <sub>x</sub> N	Particle-phase C <sub>x</sub> N
CHON <sub>2</sub>	Oxidized organic nitrogen with two nitrogen atoms	PMF	Positive matrix factorization
CIMS	Chemical ionization mass spectrometer	pON	Particle-phase organic nitrates
C <sub>others</sub> N	Oxidized organic nitrogen molecules not in the other four group	pOON	Particle-phase oxidized organic nitrogen
C <sub>x</sub> N	Oxidized organic nitrogen molecules with <i>x</i> carbon atoms	pOON <sub>AMS</sub>	Particle-phase oxidized organic nitrogen derived from aerosol mass spectrometer measurement
dV	Voltage difference	pOON <sub>CIMS</sub>	Particle-phase oxidized organic nitrogen measured by the chemical ionization mass spectrometer
dV <sub>50</sub>	The voltage at which half the signal is removed (i.e., half the iodide adducts dissociate)	pOrgNO <sub>3, AMS</sub>	Nitrate functional group from particle-phase oxidized organic nitrogen measured by the aerosol mass spectrometer
FIGAERO-I-CIMS	An iodide-adduct chemical ionization mass spectrometer equipped with the Filter Inlet for Gases and AEROSols	pOrgNO <sub>3, CIMS</sub>	Nitrate functional group in particle-phase oxidized organic nitrogen based on the data by the chemical ionization mass spectrometer
GC-MS/FID	Gas chromatography coupled with mass spectrometry and a flame ionization detector	PRIDE-GBA	Particles, Radicals, and Intermediates from oxidation of primary Emissions over the Great Bay Area
gON	Gas-phase organic nitrates	PTR-ToF-MS	Proton transfer reaction time-of-flight mass spectrometry
gOON	Gas-phase oxidized organic nitrogen	RH	Relative humidity
gOON <sub>CIMS</sub>	Gas-phase oxidized organic nitrogen measured by the chemical ionization mass spectrometer	S <sub>0</sub>	The relative signal at the weakest dV compared to the signal under operational dV
HR-ToF-AMS	High-resolution time-of-flight aerosol mass spectrometer	TD	Thermodenuder
IMR	Ion–molecule reaction region	TD-LIF	Thermal dissociation laser-induced fluorescence
MW	Molecular weight	VCP	Volatile chemical product
NO <sub>x</sub>	Sum of NO and NO <sub>2</sub>	VOCs	Volatile organic compounds

**Data availability.** The data sets used to evaluate the conclusions in the study are available at <https://doi.org/10.17632/s8s6wk32fy.1> (Cai, 2022). Figures were made with Igor Pro version 6.37 and Igor Pro version 8.04, available under the Igor Pro license (WaveMetrics, 2023; <https://www.wavemetrics.com>, last access: 1 January 2023). The more detailed data can be provided by contacting the corresponding authors.

**Supplement.** The supplement related to this article is available online at: <https://doi.org/10.5194/acp-23-8855-2023-supplement>.

**Author contributions.** YC and CY: equal contributions. YC and WH: writing, visualization and validation. YC, CY, WC, WH, YP, BW, XH, LH, SG and BY: data curation, methodology. CY, WC, WH, WS, YP, SH, JQ, SW, ChW, CaW, ZW and BY: experiment, investigation and formal analysis. WH, BY, MS and XW: conceptualization, supervision, project administration and funding acquisition.

**Competing interests.** The contact author has declared that none of the authors has any competing interests.

**Disclaimer.** Publisher's note: Copernicus Publications remains neutral with regard to jurisdictional claims in published maps and institutional affiliations.

**Acknowledgements.** This work was supported by the National Key Research and Development Program of China (grant nos. 2022YFC3701000 and 2021YFA1601800), National Natural Science Foundation of China (grant nos. 42275103, 42230701, 42121004 and 41905111), Guangdong Pearl River Talents Program (grant no. 2019QN01L948), Guangdong Foundation for Program of Science and Technology Research (grant no. 2019B121205006), Guangdong Foundation for Program of Science and Technology Research (grant no. 2020B1212060053) and State Key Laboratory of Organic Geochemistry, GIGCAS (grant nos. SKLOG2020-5 and SKLOG2020-6). Joel A. Thornton and Brett B. Palm provided helpful comments.

**Financial support.** This work was supported by the National Key Research and Development Program of China (grant nos. 2022YFC3701000 and 2021YFA1601800), the National Natural Science Foundation of China (grant nos. 42275103, 42230701, 42121004 and 41905111), the Guangdong Pearl River Talents Program (grant no. 2019QN01L948), and the Guangdong Foundation for Program of Science and Technology Research (grant nos. 2019B121205006 and 2020B1212060053).

**Review statement.** This paper was edited by Anne Perring and reviewed by two anonymous referees.

## References

- Andreae, M. O.: Soot Carbon and Excess Fine Potassium: Long-Range Transport of Combustion-Derived Aerosols, *Science*, 220, 1148–1151, <https://doi.org/10.1126/science.220.4602.1148>, 1983.
- Atkinson, R. and Arey, J.: Atmospheric Degradation of Volatile Organic Compounds, *Chem. Rev.*, 103, 4605–4638, <https://doi.org/10.1021/cr0206420>, 2003.
- Ayres, B. R., Allen, H. M., Draper, D. C., Brown, S. S., Wild, R. J., Jimenez, J. L., Day, D. A., Campuzano-Jost, P., Hu, W., de Gouw, J., Koss, A., Cohen, R. C., Duffey, K. C., Romer, P., Baumann, K., Edgerton, E., Takahama, S., Thornton, J. A., Lee, B. H., Lopez-Hilfiker, F. D., Mohr, C., Wennberg, P. O., Nguyen, T. B., Teng, A., Goldstein, A. H., Olson, K., and Fry, J. L.: Organic nitrate aerosol formation via  $\text{NO}_3$  + biogenic volatile organic compounds in the southeastern United States, *Atmos. Chem. Phys.*, 15, 13377–13392, <https://doi.org/10.5194/acp-15-13377-2015>, 2015.
- Bai, J., Sun, X., Zhang, C., Xu, Y., and Qi, C.: The OH-initiated atmospheric reaction mechanism and kinetics for levoglucosan emitted in biomass burning, *Chemosphere*, 93, 2004–2010, <https://doi.org/10.1016/j.chemosphere.2013.07.021>, 2013.
- Bannan, T. J., Le Breton, M., Priestley, M., Worrall, S. D., Bacak, A., Marsden, N. A., Mehra, A., Hammes, J., Hallquist, M., Alfarra, M. R., Krieger, U. K., Reid, J. P., Jayne, J., Robinson, W., McFiggans, G., Coe, H., Percival, C. J., and Topping, D.: A method for extracting calibrated volatility information from the FIGAERO-HR-ToF-CIMS and its experimental application, *Atmos. Meas. Tech.*, 12, 1429–1439, <https://doi.org/10.5194/amt-12-1429-2019>, 2019.
- Bell, D. M., Wu, C., Bertrand, A., Graham, E., Schoonbaert, J., Giannoukos, S., Baltensperger, U., Prevot, A. S. H., Riipinen, I., El Haddad, I., and Mohr, C.: Particle-phase processing of  $\alpha$ -pinene  $\text{NO}_3$  secondary organic aerosol in the dark, *Atmos. Chem. Phys.*, 22, 13167–13182, <https://doi.org/10.5194/acp-22-13167-2022>, 2022.
- Bhattacharai, H., Saikawa, E., Wan, X., Zhu, H., Ram, K., Gao, S., Kang, S., Zhang, Q., Zhang, Y., Wu, G., Wang, X., Kawamura, K., Fu, P., and Cong, Z.: Levoglucosan as a tracer of biomass burning: Recent progress and perspectives, *Atmos. Res.*, 220, 20–33, <https://doi.org/10.1016/j.atmosres.2019.01.004>, 2019.
- Bi, C., Krechmer, J. E., Frazier, G. O., Xu, W., Lambe, A. T., Claffin, M. S., Lerner, B. M., Jayne, J. T., Worsnop, D. R., Canagaratna, M. R., and Isaacman-VanWertz, G.: Coupling a gas chromatograph simultaneously to a flame ionization detector and chemical ionization mass spectrometer for isomer-resolved measurements of particle-phase organic compounds, *Atmos. Meas. Tech.*, 14, 3895–3907, <https://doi.org/10.5194/amt-14-3895-2021>, 2021a.
- Bi, C., Krechmer, J. E., Frazier, G. O., Xu, W., Lambe, A. T., Claffin, M. S., Lerner, B. M., Jayne, J. T., Worsnop, D. R., Canagaratna, M. R., and Isaacman-VanWertz, G.: Quantification of isomer-resolved iodide chemical ionization mass spectrometry sensitivity and uncertainty using a voltage-scanning approach, *Atmos. Meas. Tech.*, 14, 6835–6850, <https://doi.org/10.5194/amt-14-6835-2021>, 2021b.
- Brown, S. S. and Stutz, J.: Nighttime radical observations and chemistry, *Chem. Soc. Rev.*, 41, 6405–6447, <https://doi.org/10.1039/c2cs35181a>, 2012.

- Brownwood, B., Turdziladze, A., Hohaus, T., Wu, R., Mentel, T. F., Carlsson, P. T. M., Tsiligiannis, E., Hallquist, M., Andres, S., Hantschke, L., Reimer, D., Rohrer, F., Tillmann, R., Winter, B., Liebmann, J., Brown, S. S., Kiendler-Scharr, A., Novelli, A., Fuchs, H., and Fry, J. L.: Gas-Particle Partitioning and SOA Yields of Organonitrate Products from NO<sub>3</sub>-Initiated Oxidation of Isoprene under Varied Chemical Regimes, *ACS Earth Space Chem.*, 5, 785–800, <https://doi.org/10.1021/acsearthspacechem.0c00311>, 2021.
- Cai, Y.: 2022\_0608\_PRIDEGBA\_Dataset\_cyy\_v3, V1, Mendeley Data [data set], <https://doi.org/10.17632/s8s6wk32fy.1>, 2022.
- Canagaratna, M. R., Jayne, J. T., Jimenez, J. L., Allan, J. D., Alfarra, M. R., Zhang, Q., Onasch, T. B., Drewnick, F., Coe, H., Middlebrook, A., Delia, A., Williams, L. R., Trimborn, A. M., Northway, M. J., DeCarlo, P. F., Kolb, C. E., Davidovits, P., and Worsnop, D. R.: Chemical and microphysical characterization of ambient aerosols with the aerodyne aerosol mass spectrometer, *Mass Spectrom. Rev.*, 26, 185–222, <https://doi.org/10.1002/mas.20115>, 2007.
- Capouet, M. and Müller, J.-F.: A group contribution method for estimating the vapour pressures of  $\alpha$ -pinene oxidation products, *Atmos. Chem. Phys.*, 6, 1455–1467, <https://doi.org/10.5194/acp-6-1455-2006>, 2006.
- Chen, W., Ye, Y. Q., Hu, W. W., Zhou, H. S., Pan, T. L., Wang, Y. K., Song, W., Song, Q. C., Ye, C. S., Wang, C. M., Wang, B. L., Huang, S., Yuan, B., Zhu, M., Lian, X. F., Zhang, G. H., Bi, X. H., Jiang, F., Liu, J. W., Canonaco, F., Prevot, A. S. H., Shao, M., and Wang, X. M.: Real-Time Characterization of Aerosol Compositions, Sources, and Aging Processes in Guangzhou During PRIDE-GBA 2018 Campaign, *J. Geophys. Res.-Atmos.*, 126, e2021JD035114, <https://doi.org/10.1029/2021JD035114>, 2021.
- Chen, X., Wang, H., and Lu, K.: Interpretation of NO<sub>3</sub>-N<sub>2</sub>O<sub>5</sub> observation via steady state in high-aerosol air mass: the impact of equilibrium coefficient in ambient conditions, *Atmos. Chem. Phys.*, 22, 3525–3533, <https://doi.org/10.5194/acp-22-3525-2022>, 2022.
- Chen, Y., Takeuchi, M., Nah, T., Xu, L., Canagaratna, M. R., Stark, H., Baumann, K., Canonaco, F., Prévôt, A. S. H., Huey, L. G., Weber, R. J., and Ng, N. L.: Chemical characterization of secondary organic aerosol at a rural site in the southeastern US: insights from simultaneous high-resolution time-of-flight aerosol mass spectrometer (HR-ToF-AMS) and FIGAERO chemical ionization mass spectrometer (CIMS) measurements, *Atmos. Chem. Phys.*, 20, 8421–8440, <https://doi.org/10.5194/acp-20-8421-2020>, 2020.
- Chen, Y., Zheng, P., Wang, Z., Pu, W., Tan, Y., Yu, C., Xia, M., Wang, W., Guo, J., Huang, D., Yan, C., Nie, W., Ling, Z., Chen, Q., Lee, S., and Wang, T.: Secondary Formation and Impacts of Gaseous Nitro-Phenolic Compounds in the Continental Outflow Observed at a Background Site in South China, *Environ. Sci. Technol.*, 56, 6933–6943, <https://doi.org/10.1021/acs.est.1c04596>, 2022.
- Cheng, Y., Engling, G., He, K.-B., Duan, F.-K., Ma, Y.-L., Du, Z.-Y., Liu, J.-M., Zheng, M., and Weber, R. J.: Biomass burning contribution to Beijing aerosol, *Atmos. Chem. Phys.*, 13, 7765–7781, <https://doi.org/10.5194/acp-13-7765-2013>, 2013.
- Coggon, M. M., Gkatzelis, G. I., McDonald, B. C., Gilman, J. B., Schwantes, R. H., Abuhassan, N., Aikin, K. C., Arend, M. F., Berkoff, T. A., Brown, S. S., Campos, T. L., Dickerson, R. R., Gronoff, G., Hurley, J. F., Isaacman-VanWertz, G., Koss, A. R., Li, M., McKeen, S. A., Moshary, F., Peischl, J., Pospisilova, V., Ren, X., Wilson, A., Wu, Y., Trainer, M., and Warneke, C.: Volatile chemical product emissions enhance ozone and modulate urban chemistry, *P. Natl. Acad. Sci. USA*, 118, e2026653118, <https://doi.org/10.1073/pnas.2026653118>, 2021.
- Cubison, M. J., Ortega, A. M., Hayes, P. L., Farmer, D. K., Day, D., Lechner, M. J., Brune, W. H., Apel, E., Diskin, G. S., Fisher, J. A., Fuelberg, H. E., Hecobian, A., Knapp, D. J., Mikoviny, T., Riemer, D., Sachse, G. W., Sessions, W., Weber, R. J., Weinheimer, A. J., Wisthaler, A., and Jimenez, J. L.: Effects of aging on organic aerosol from open biomass burning smoke in aircraft and laboratory studies, *Atmos. Chem. Phys.*, 11, 12049–12064, <https://doi.org/10.5194/acp-11-12049-2011>, 2011.
- Dancey, C. P. and Reidy, J.: *Statistics Without Maths for Psychology*, 4th edn., Pearson/Prentice Hall, Harlow, England, New York, ISBN 9780132051606, 2007.
- Day, D. A., Liu, S., Russell, L. M., and Ziemann, P. J.: Organonitrate group concentrations in submicron particles with high nitrate and organic fractions in coastal southern California, *Atmos. Environ.*, 44, 1970–1979, <https://doi.org/10.1016/j.atmosenv.2010.02.045>, 2010.
- Day, D. A., Wooldridge, P. J., Dillon, M. B., Thornton, J. A., and Cohen, R. C.: A thermal dissociation laser-induced fluorescence instrument for in situ detection of NO<sub>2</sub>, peroxy nitrates, alkyl nitrates, and HNO<sub>3</sub>, *J. Geophys. Res.-Atmos.*, 107, ACH 4-1–ACH 4-14, <https://doi.org/10.1029/2001jd000779>, 2002.
- Day, D. A., Campuzano-Jost, P., Nault, B. A., Palm, B. B., Hu, W., Guo, H., Wooldridge, P. J., Cohen, R. C., Docherty, K. S., Huffman, J. A., de Sá, S. S., Martin, S. T., and Jimenez, J. L.: A systematic re-evaluation of methods for quantification of bulk particle-phase organic nitrates using real-time aerosol mass spectrometry, *Atmos. Meas. Tech.*, 15, 459–483, <https://doi.org/10.5194/amt-15-459-2022>, 2022.
- DeCarlo, P. F., Kimmel, J. R., Trimborn, A., Northway, M. J., Jayne, J. T., Aiken, A. C., Gonin, M., Fuhrer, K., Horvath, T., Docherty, K. S., Worsnop, D. R., and Jimenez, J. L.: Field-Deployable, High-Resolution, Time-of-Flight Aerosol Mass Spectrometer, *Anal. Chem.*, 78, 8281–8289, <https://doi.org/10.1021/ac061249n>, 2006.
- de Gouw, J. A., Warneke, C., Stohl, A., Holloway, J., Trainer, M., and Fehsenfeld, F. C.: Emissions and Photochemistry of Oxygenated VOCs in the Outflow from Urban Centers in the Northeastern U.S., *AGU Fall Meeting Abstracts*, Moscone Convention Center West, 800 Howard Street, San Francisco, December 2005, A31E-05, <https://ui.adsabs.harvard.edu/abs/2005AGUFM.A31E..05D> (last access: 17 July 2023), 2005.
- Ditto, J. C., Machesky, J., and Gentner, D. R.: Analysis of reduced and oxidized nitrogen-containing organic compounds at a coastal site in summer and winter, *Atmos. Chem. Phys.*, 22, 3045–3065, <https://doi.org/10.5194/acp-22-3045-2022>, 2022.
- Farmer, D. K., Matsunaga, A., Docherty, K. S., Surratt, J. D., Seinfeld, J. H., Ziemann, P. J., and Jimenez, J. L.: Response of an aerosol mass spectrometer to organonitrates and organosulfates and implications for atmospheric chemistry, *P. Natl. Acad. Sci. USA*, 107, 6670–6675, <https://doi.org/10.1073/pnas.0912340107>, 2010.
- Farmer, D. K., Perring, A. E., Wooldridge, P. J., Blake, D. R., Baker, A., Meinardi, S., Huey, L. G., Tanner, D., Vargas, O., and Cohen,

- R. C.: Impact of organic nitrates on urban ozone production, *Atmos. Chem. Phys.*, 11, 4085–4094, <https://doi.org/10.5194/acp-11-4085-2011>, 2011.
- Faxon, C., Hammes, J., Le Breton, M., Pathak, R. K., and Halquist, M.: Characterization of organic nitrate constituents of secondary organic aerosol (SOA) from nitrate-radical-initiated oxidation of limonene using high-resolution chemical ionization mass spectrometry, *Atmos. Chem. Phys.*, 18, 5467–5481, <https://doi.org/10.5194/acp-18-5467-2018>, 2018.
- Fisher, J. A., Jacob, D. J., Travis, K. R., Kim, P. S., Marais, E. A., Chan Miller, C., Yu, K., Zhu, L., Yantosca, R. M., Sulprizio, M. P., Mao, J., Wennberg, P. O., Crouse, J. D., Teng, A. P., Nguyen, T. B., St. Clair, J. M., Cohen, R. C., Romer, P., Nault, B. A., Wooldridge, P. J., Jimenez, J. L., Campuzano-Jost, P., Day, D. A., Hu, W., Shepson, P. B., Xiong, F., Blake, D. R., Goldstein, A. H., Misztal, P. K., Hanisco, T. F., Wolfe, G. M., Ryerson, T. B., Wisthaler, A., and Mikoviny, T.: Organic nitrate chemistry and its implications for nitrogen budgets in an isoprene- and monoterpene-rich atmosphere: constraints from aircraft (SEAC4RS) and ground-based (SOAS) observations in the Southeast US, *Atmos. Chem. Phys.*, 16, 5969–5991, <https://doi.org/10.5194/acp-16-5969-2016>, 2016.
- Fry, J. L., Draper, D. C., Zarzana, K. J., Campuzano-Jost, P., Day, D. A., Jimenez, J. L., Brown, S. S., Cohen, R. C., Kaser, L., Hansel, A., Cappellin, L., Karl, T., Hodzic Roux, A., Turnipseed, A., Cantrell, C., Lefer, B. L., and Grossberg, N.: Observations of gas- and aerosol-phase organic nitrates at BEACHON-RoMBAS 2011, *Atmos. Chem. Phys.*, 13, 8585–8605, <https://doi.org/10.5194/acp-13-8585-2013>, 2013.
- Gaston, C. J., Lopez-Hilfiker, F. D., Whybrew, L. E., Hadley, O., McNair, F., Gao, H., Jaffe, D. A., and Thornton, J. A.: Online molecular characterization of fine particulate matter in Port Angeles, WA: Evidence for a major impact from residential wood smoke, *Atmos. Environ.*, 138, 99–107, <https://doi.org/10.1016/j.atmosenv.2016.05.013>, 2016.
- George, C., Ammann, M., D’Anna, B., Donaldson, D. J., and Nizkorodov, S. A.: Heterogeneous photochemistry in the atmosphere, *Chem. Rev.*, 115, 4218–4258, <https://doi.org/10.1021/cr500648z>, 2015.
- George, I. J. and Abbatt, J. P.: Heterogeneous oxidation of atmospheric aerosol particles by gas-phase radicals, *Nat. Chem.*, 2, 713–722, <https://doi.org/10.1038/nchem.806>, 2010.
- Gilman, J. B., Lerner, B. M., Kuster, W. C., Goldan, P. D., Warneke, C., Veres, P. R., Roberts, J. M., de Gouw, J. A., Burling, I. R., and Yokelson, R. J.: Biomass burning emissions and potential air quality impacts of volatile organic compounds and other trace gases from fuels common in the US, *Atmos. Chem. Phys.*, 15, 13915–13938, <https://doi.org/10.5194/acp-15-13915-2015>, 2015.
- Gkatzelis, G. I., Coggon, M. M., McDonald, B. C., Peischl, J., Aikin, K. C., Gilman, J. B., Trainer, M., and Warneke, C.: Identifying Volatile Chemical Product Tracer Compounds in U.S. Cities, *Environ. Sci. Technol.*, 55, 188–199, <https://doi.org/10.1021/acs.est.0c05467>, 2021.
- Gross, S., Iannone, R., Xiao, S., and Bertram, A. K.: Reactive uptake studies of NO<sub>3</sub> and N<sub>2</sub>O<sub>5</sub> on alkenoic acid, alkanolate, and polyalcohol substrates to probe nighttime aerosol chemistry, *Phys. Chem. Chem. Phys.*, 11, 7792–7803, <https://doi.org/10.1039/B904741G>, 2009.
- Hamilton, J. F., Bryant, D. J., Edwards, P. M., Ouyang, B., Bannan, T. J., Mehra, A., Mayhew, A. W., Hopkins, J. R., Dunmore, R. E., Squires, F. A., Lee, J. D., Newland, M. J., Worrall, S. D., Bacak, A., Coe, H., Percival, C., Whalley, L. K., Heard, D. E., Slater, E. J., Jones, R. L., Cui, T., Surratt, J. D., Reeves, C. E., Mills, G. P., Grimmond, S., Sun, Y., Xu, W., Shi, Z., and Rickard, A. R.: Key Role of NO<sub>3</sub> Radicals in the Production of Isoprene Nitrates and Nitrooxyorganosulfates in Beijing, *Environ. Sci. Technol.*, 55, 842–853, <https://doi.org/10.1021/acs.est.0c05689>, 2021.
- Hao, L. Q., Kortelainen, A., Romakkaniemi, S., Portin, H., Jaatinen, A., Leskinen, A., Komppula, M., Miettinen, P., Sueper, D., Pajunaja, A., Smith, J. N., Lehtinen, K. E. J., Worsnop, D. R., Laaksonen, A., and Virtanen, A.: Atmospheric submicron aerosol composition and particulate organic nitrate formation in a boreal forestland–urban mixed region, *Atmos. Chem. Phys.*, 14, 13483–13495, <https://doi.org/10.5194/acp-14-13483-2014>, 2014.
- Harrison, R. M., Tilling, R., Callén Romero, M. A. S., Harrad, S., and Jarvis, K.: A study of trace metals and polycyclic aromatic hydrocarbons in the roadside environment, *Atmos. Environ.*, 37, 2391–2402, [https://doi.org/10.1016/S1352-2310\(03\)00122-5](https://doi.org/10.1016/S1352-2310(03)00122-5), 2003.
- He, Q., Tomaz, S., Li, C., Zhu, M., Meidan, D., Riva, M., Laskin, A., Brown, S. S., George, C., Wang, X., and Rudich, Y.: Optical Properties of Secondary Organic Aerosol Produced by Nitrate Radical Oxidation of Biogenic Volatile Organic Compounds, *Environ. Sci. Technol.*, 55, 2878–2889, <https://doi.org/10.1021/acs.est.0c06838>, 2021.
- Hellén, H., Tykkä, T., and Hakola, H.: Importance of monoterpenes and isoprene in urban air in northern Europe, *Atmos. Environ.*, 59, 59–66, <https://doi.org/10.1016/j.atmosenv.2012.04.049>, 2012.
- Hennigan, C. J., Sullivan, A. P., Collett, J. L., and Robinson, A. L.: Levoglucosan stability in biomass burning particles exposed to hydroxyl radicals, *Geophys. Res. Lett.*, 37, L09806, <https://doi.org/10.1029/2010gl043088>, 2010.
- Hilas, C. S., Goudos, S. K., and Sahalos, J. N.: Seasonal decomposition and forecasting of telecommunication data: A comparative case study, *Technol. Forecast. Soc.*, 73, 495–509, <https://doi.org/10.1016/j.techfore.2005.07.002>, 2006.
- Hoffmann, D., Tilgner, A., Iinuma, Y., and Herrmann, H.: Atmospheric Stability of Levoglucosan: A Detailed Laboratory and Modeling Study, *Environ. Sci. Technol.*, 44, 694–699, <https://doi.org/10.1021/es902476f>, 2010.
- Huang, W., Saathoff, H., Shen, X., Ramisetty, R., Leisner, T., and Mohr, C.: Chemical Characterization of Highly Functionalized Organonitrates Contributing to Night-Time Organic Aerosol Mass Loadings and Particle Growth, *Environ. Sci. Technol.*, 53, 1165–1174, <https://doi.org/10.1021/acs.est.8b05826>, 2019.
- Isaacman-VanWertz, G., Massoli, P., O’Brien, R., Lim, C., Franklin, J. P., Moss, J. A., Hunter, J. F., Nowak, J. B., Canagaratna, M. R., Misztal, P. K., Arata, C., Roscioli, J. R., Herndon, S. T., Onasch, T. B., Lambe, A. T., Jayne, J. T., Su, L., Knopf, D. A., Goldstein, A. H., Worsnop, D. R., and Kroll, J. H.: Chemical evolution of atmospheric organic carbon over multiple generations of oxidation, *Nat. Chem.*, 10, 462–468, <https://doi.org/10.1038/s41557-018-0002-2>, 2018.
- Iyer, S., Lopez-Hilfiker, F., Lee, B. H., Thornton, J. A., and Kurtén, T.: Modeling the Detection of Organic and Inorganic Compounds

- Using Iodide-Based Chemical Ionization, *J. Phys. Chem. A*, 120, 576–587, <https://doi.org/10.1021/acs.jpca.5b09837>, 2016.
- Iyer, S., Rissanen, M. P., Valiev, R., Barua, S., Krechmer, J. E., Thornton, J., Ehn, M., and Kurtén, T.: Molecular mechanism for rapid autoxidation in  $\alpha$ -pinene ozonolysis, *Nat. Commun.*, 12, 878, <https://doi.org/10.1038/s41467-021-21172-w>, 2021.
- Jiang, F., Liu, J., Cheng, Z., Ding, P., Zhu, S., Yuan, X., Chen, W., Zhang, Z., Zong, Z., Tian, C., Hu, W., Zheng, J., Szidat, S., Li, J., and Zhang, G.: Quantitative evaluation for the sources and aging processes of organic aerosols in urban Guangzhou: Insights from a comprehensive method of dual-carbon isotopes and macro tracers, *Sci. Total Environ.*, 888, 164182, <https://doi.org/10.1016/j.scitotenv.2023.164182>, 2023.
- Juncosa Calahorrano, J. F., Lindaas, J., O'Dell, K., Palm, B. B., Peng, Q., Flocke, F., Pollack, I. B., Garofalo, L. A., Farmer, D. K., Pierce, J. R., Collett Jr, J. L., Weinheimer, A., Campos, T., Hornbrook, R. S., Hall, S. R., Ullmann, K., Pothier, M. A., Apel, E. C., Permar, W., Hu, L., Hills, A. J., Montzka, D., Tyndall, G., Thornton, J. A., and Fischer, E. V.: Daytime Oxidized Reactive Nitrogen Partitioning in Western U.S. Wildfire Smoke Plumes, *J. Geophys. Res.-Atmos.*, 126, e2020JD033484, <https://doi.org/10.1029/2020JD033484>, 2021.
- Keehan, N. I., Brownwood, B., Marsavin, A., Day, D. A., and Fry, J. L.: A thermal-dissociation-cavity ring-down spectrometer (TD-CRDS) for the detection of organic nitrates in gas and particle phases, *Atmos. Meas. Tech.*, 13, 6255–6269, <https://doi.org/10.5194/amt-13-6255-2020>, 2020.
- Kiendler-Scharr, A., Mensah, A. A., Friese, E., Topping, D., Nemitz, E., Prevot, A. S. H., Äijälä, M., Allan, J., Canonaco, F., Canagaratna, M., Carbone, S., Crippa, M., Dall'Osto, M., Day, D. A., De Carlo, P., Di Marco, C. F., Elbern, H., Eriksson, A., Freney, E., Hao, L., Herrmann, H., Hildebrandt, L., Hillamo, R., Jimenez, J. L., Laaksonen, A., McFiggans, G., Mohr, C., O'Dowd, C., Otjes, R., Ovadnevaite, J., Pandis, S. N., Poulain, L., Schlag, P., Sellegri, K., Swietlicki, E., Tiitta, P., Vermeulen, A., Wahner, A., Worsnop, D., and Wu, H. C.: Ubiquity of organic nitrates from nighttime chemistry in the European submicron aerosol, *Geophys. Res. Lett.*, 43, 7735–7744, <https://doi.org/10.1002/2016gl069239>, 2016.
- Koch, B. P. and Dittmar, T.: From mass to structure: an aromaticity index for high-resolution mass data of natural organic matter, *Rapid Commun. Mass Spectrom.*, 20, 926–932, <https://doi.org/10.1002/rcm.2386>, 2006.
- Koch, B. P. and Dittmar, T.: From mass to structure: an aromaticity index for high-resolution mass data of natural organic matter, *Rapid Commun. Mass Spectrom.*, 30, 250–250, <https://doi.org/10.1002/rcm.7433>, 2016.
- Kodros, J. K., Papanastasiou, D. K., Paglione, M., Masiol, M., Squizzato, S., Florou, K., Skyllakou, K., Kaltsonoudis, C., Nenes, A., and Pandis, S. N.: Rapid dark aging of biomass burning as an overlooked source of oxidized organic aerosol, *P. Natl. Acad. Sci. USA*, 117, 33028–33033, <https://doi.org/10.1073/pnas.2010365117>, 2020.
- Kroll, J. H. and Seinfeld, J. H.: Chemistry of secondary organic aerosol: Formation and evolution of low-volatility organics in the atmosphere, *Atmos. Environ.*, 42, 3593–3624, <https://doi.org/10.1016/j.atmosenv.2008.01.003>, 2008.
- Lai, C., Liu, Y., Ma, J., Ma, Q., and He, H.: Degradation kinetics of levoglucosan initiated by hydroxyl radical under different environmental conditions, *Atmos. Environ.*, 91, 32–39, <https://doi.org/10.1016/j.atmosenv.2014.03.054>, 2014.
- Le Breton, M., Psichoudaki, M., Hallquist, M., Watne, Å. K., Lutz, A., and Hallquist, Å. M.: Application of a FIGAERO ToF CIMS for on-line characterization of real-world fresh and aged particle emissions from buses, *Aerosol Sci. Technol.*, 53, 244–259, <https://doi.org/10.1080/02786826.2019.1566592>, 2019.
- Lee, B. H., Lopez-Hilfiker, F. D., Mohr, C., Kurtén, T., Worsnop, D. R., and Thornton, J. A.: An iodide-adduct high-resolution time-of-flight chemical-ionization mass spectrometer: application to atmospheric inorganic and organic compounds, *Environ. Sci. Technol.*, 48, 6309–6317, <https://doi.org/10.1021/es500362a>, 2014.
- Lee, B. H., Mohr, C., Lopez-Hilfiker, F. D., Lutz, A., Hallquist, M., Lee, L., Romer, P., Cohen, R. C., Iyer, S., Kurtén, T., Hu, W., Day, D. A., Campuzano-Jost, P., Jimenez, J. L., Xu, L., Ng, N. L., Guo, H., Weber, R. J., Wild, R. J., Brown, S. S., Koss, A., de Gouw, J., Olson, K., Goldstein, A. H., Seco, R., Kim, S., McAvey, K., Shepson, P. B., Starn, T., Baumann, K., Edgerton, E. S., Liu, J., Shilling, J. E., Miller, D. O., Brune, W., Schobesberger, S., D'Ambro, E. L., and Thornton, J. A.: Highly functionalized organic nitrates in the southeast United States: Contribution to secondary organic aerosol and reactive nitrogen budgets, *P. Natl. Acad. Sci. USA*, 113, 1516–1521, <https://doi.org/10.1073/pnas.1508108113>, 2016.
- Lee, B. H., Lopez-Hilfiker, F. D., D'Ambro, E. L., Zhou, P., Boy, M., Petäjä, T., Hao, L., Virtanen, A., and Thornton, J. A.: Semi-volatile and highly oxygenated gaseous and particulate organic compounds observed above a boreal forest canopy, *Atmos. Chem. Phys.*, 18, 11547–11562, <https://doi.org/10.5194/acp-18-11547-2018>, 2018.
- Lee, C. P., Surdu, M., Bell, D. M., Lamkaddam, H., Wang, M., Ataei, F., Hofbauer, V., Lopez, B., Donahue, N. M., Dommen, J., Prevot, A. S. H., Slowik, J. G., Wang, D., Baltensperger, U., and El Haddad, I.: Effects of aerosol size and coating thickness on the molecular detection using extractive electrospray ionization, *Atmos. Meas. Tech.*, 14, 5913–5923, <https://doi.org/10.5194/amt-14-5913-2021>, 2021.
- Lee, L., Wooldridge, P. J., deGouw, J., Brown, S. S., Bates, T. S., Quinn, P. K., and Cohen, R. C.: Particulate organic nitrates observed in an oil and natural gas production region during wintertime, *Atmos. Chem. Phys.*, 15, 9313–9325, <https://doi.org/10.5194/acp-15-9313-2015>, 2015.
- Li, T., Wang, Z., Yuan, B., Ye, C., Lin, Y., Wang, S., Sha, Q. e., Yuan, Z., Zheng, J., and Shao, M.: Emissions of carboxylic acids, hydrogen cyanide (HCN) and isocyanic acid (HNCO) from vehicle exhaust, *Atmos. Environ.*, 247, 118218, <https://doi.org/10.1016/j.atmosenv.2021.118218>, 2021a.
- Li, X.-B., Yuan, B., Wang, S., Wang, C., Lan, J., Liu, Z., Song, Y., He, X., Huangfu, Y., Pei, C., Cheng, P., Yang, S., Qi, J., Wu, C., Huang, S., You, Y., Chang, M., Zheng, H., Yang, W., Wang, X., and Shao, M.: Variations and sources of volatile organic compounds (VOCs) in urban region: insights from measurements on a tall tower, *Atmos. Chem. Phys.*, 22, 10567–10587, <https://doi.org/10.5194/acp-22-10567-2022>, 2022.
- Li, Y., Fu, T. M., Yu, J. Z., Feng, X., Zhang, L., Chen, J., Boreddy, S. K. R., Kawamura, K., Fu, P., Yang, X., Zhu, L., and Zeng, Z.: Impacts of Chemical Degradation on the Global Budget of Atmospheric Levoglucosan and Its Use As a

- Biomass Burning Tracer, *Environ. Sci. Technol.*, **55**, 5525–5536, <https://doi.org/10.1021/acs.est.0c07313>, 2021b.
- Liebmann, J., Sobanski, N., Schuladen, J., Karu, E., Hellén, H., Hakola, H., Zha, Q., Ehn, M., Riva, M., Heikkinen, L., Williams, J., Fischer, H., Lelieveld, J., and Crowley, J. N.: Alkyl nitrates in the boreal forest: formation via the NO<sub>3</sub>-, OH- and O<sub>3</sub>-induced oxidation of biogenic volatile organic compounds and ambient lifetimes, *Atmos. Chem. Phys.*, **19**, 10391–10403, <https://doi.org/10.5194/acp-19-10391-2019>, 2019.
- Lim, Y. B. and Ziemann, P. J.: Chemistry of Secondary Organic Aerosol Formation from OH Radical-Initiated Reactions of Linear, Branched, and Cyclic Alkanes in the Presence of NO<sub>x</sub>, *Aerosol Sci. Technol.*, **43**, 604–619, <https://doi.org/10.1080/02786820902802567>, 2009.
- Lin, P., Bluvshstein, N., Rudich, Y., Nizkorodov, S. A., Laskin, J., and Laskin, A.: Molecular Chemistry of Atmospheric Brown Carbon Inferred from a Nationwide Biomass Burning Event, *Environ. Sci. Technol.*, **51**, 11561–11570, <https://doi.org/10.1021/acs.est.7b02276>, 2017.
- Liu, X., Huey, L. G., Yokelson, R. J., Selimovic, V., Simpson, I. J., Müller, M., Jimenez, J. L., Campuzano-Jost, P., Beyersdorf, A. J., Blake, D. R., Butterfield, Z., Choi, Y., Crouse, J. D., Day, D. A., Diskin, G. S., Dubey, M. K., Fortner, E., Hanisco, T. F., Hu, W., King, L. E., Kleinman, L., Meinardi, S., Mikoviny, T., Onasch, T. B., Palm, B. B., Peischl, J., Pollack, I. B., Ryerson, T. B., Sachse, G. W., Sedlacek, A. J., Shilling, J. E., Springston, S., St. Clair, J. M., Tanner, D. J., Teng, A. P., Wennberg, P. O., Wisthaler, A., and Wolfe, G. M.: Airborne measurements of western U.S. wildfire emissions: Comparison with prescribed burning and air quality implications, *J. Geophys. Res.-Atmos.*, **122**, 6108–6129, <https://doi.org/10.1002/2016jd026315>, 2017.
- Liu, X., Deming, B., Pagonis, D., Day, D. A., Palm, B. B., Talukdar, R., Roberts, J. M., Veres, P. R., Krechmer, J. E., Thornton, J. A., de Gouw, J. A., Ziemann, P. J., and Jimenez, J. L.: Effects of gas-wall interactions on measurements of semivolatile compounds and small polar molecules, *Atmos. Meas. Tech.*, **12**, 3137–3149, <https://doi.org/10.5194/amt-12-3137-2019>, 2019.
- Lopez-Hilfiker, F. D., Mohr, C., Ehn, M., Rubach, F., Kleist, E., Wildt, J., Mentel, Th. F., Lutz, A., Hallquist, M., Worsnop, D., and Thornton, J. A.: A novel method for online analysis of gas and particle composition: description and evaluation of a Filter Inlet for Gases and AEROSols (FIGAERO), *Atmos. Meas. Tech.*, **7**, 983–1001, <https://doi.org/10.5194/amt-7-983-2014>, 2014.
- Lopez-Hilfiker, F. D., Iyer, S., Mohr, C., Lee, B. H., D'Ambro, E. L., Kurtén, T., and Thornton, J. A.: Constraining the sensitivity of iodide adduct chemical ionization mass spectrometry to multifunctional organic molecules using the collision limit and thermodynamic stability of iodide ion adducts, *Atmos. Meas. Tech.*, **9**, 1505–1512, <https://doi.org/10.5194/amt-9-1505-2016>, 2016.
- Lopez-Hilfiker, F. D., Pospisilova, V., Huang, W., Kalberer, M., Mohr, C., Stefenelli, G., Thornton, J. A., Baltensperger, U., Prevot, A. S. H., and Slowik, J. G.: An extractive electrospray ionization time-of-flight mass spectrometer (EESI-TOF) for online measurement of atmospheric aerosol particles, *Atmos. Meas. Tech.*, **12**, 4867–4886, <https://doi.org/10.5194/amt-12-4867-2019>, 2019.
- Mao, J., Ren, X., Brune, W. H., Olson, J. R., Crawford, J. H., Fried, A., Huey, L. G., Cohen, R. C., Heikes, B., Singh, H. B., Blake, D. R., Sachse, G. W., Diskin, G. S., Hall, S. R., and Shetter, R. E.: Airborne measurement of OH reactivity during INTEX-B, *Atmos. Chem. Phys.*, **9**, 163–173, <https://doi.org/10.5194/acp-9-163-2009>, 2009.
- Matsunaga, A. and Ziemann, P. J.: Yields of beta-hydroxynitrates, dihydroxynitrates, and trihydroxynitrates formed from OH radical-initiated reactions of 2-methyl-1-alkenes, *P. Natl. Acad. Sci. USA*, **107**, 6664–6669, <https://doi.org/10.1073/pnas.0910585107>, 2010.
- Mayhew, A. W., Lee, B. H., Thornton, J. A., Bannan, T. J., Brean, J., Hopkins, J. R., Lee, J. D., Nelson, B. S., Percival, C., Rickard, A. R., Shaw, M. D., Edwards, P. M., and Hamilton, J. F.: Evaluation of isoprene nitrate chemistry in detailed chemical mechanisms, *Atmos. Chem. Phys.*, **22**, 14783–14798, <https://doi.org/10.5194/acp-22-14783-2022>, 2022.
- Mayorga, R., Xia, Y., Zhao, Z., Long, B., and Zhang, H.: Peroxy Radical Autoxidation and Sequential Oxidation in Organic Nitrate Formation during Limonene Night-time Oxidation, *Environ. Sci. Technol.*, **56**, 15337–15346, <https://doi.org/10.1021/acs.est.2c04030>, 2022.
- Mohr, C., Huffman, J. A., Cubison, M. J., Aiken, A. C., Docherty, K. S., Kimmel, J. R., Ulbrich, I. M., Hannigan, M., and Jimenez, J. L.: Characterization of Primary Organic Aerosol Emissions from Meat Cooking, Trash Burning, and Motor Vehicles with High-Resolution Aerosol Mass Spectrometry and Comparison with Ambient and Chamber Observations, *Environ. Sci. Technol.*, **43**, 2443–2449, <https://doi.org/10.1021/es8011518>, 2009.
- Mohr, C., Lopez-Hilfiker, F. D., Zotter, P., Prévôt, A. S. H., Xu, L., Ng, N. L., Herndon, S. C., Williams, L. R., Franklin, J. P., Zahniser, M. S., Worsnop, D. R., Knighton, W. B., Aiken, A. C., Gorkowski, K. J., Dubey, M. K., Allan, J. D., and Thornton, J. A.: Contribution of Nitrated Phenols to Wood Burning Brown Carbon Light Absorption in Detling, United Kingdom during Winter Time, *Environ. Sci. Technol.*, **47**, 6316–6324, <https://doi.org/10.1021/es400683v>, 2013.
- Ng, N. L., Brown, S. S., Archibald, A. T., Atlas, E., Cohen, R. C., Crowley, J. N., Day, D. A., Donahue, N. M., Fry, J. L., Fuchs, H., Griffin, R. J., Guzman, M. I., Herrmann, H., Hodzic, A., Iinuma, Y., Jimenez, J. L., Kiendler-Scharr, A., Lee, B. H., Luecken, D. J., Mao, J., McLaren, R., Mutzel, A., Osthoff, H. D., Ouyang, B., Picquet-Varrault, B., Platt, U., Pye, H. O. T., Rudich, Y., Schwantes, R. H., Shiraiwa, M., Stutz, J., Thornton, J. A., Tilgner, A., Williams, B. J., and Zaveri, R. A.: Nitrate radicals and biogenic volatile organic compounds: oxidation, mechanisms, and organic aerosol, *Atmos. Chem. Phys.*, **17**, 2103–2162, <https://doi.org/10.5194/acp-17-2103-2017>, 2017.
- Odum, J. R., Hoffmann, T., Bowman, F., Collins, D., Flagan, R. C., and Seinfeld, J. H.: Gas/Particle Partitioning and Secondary Organic Aerosol Yields, *Environ. Sci. Technol.*, **30**, 2580–2585, <https://doi.org/10.1021/es950943+>, 1996.
- Pagonis, D., Krechmer, J. E., de Gouw, J., Jimenez, J. L., and Ziemann, P. J.: Effects of gas-wall partitioning in Teflon tubing and instrumentation on time-resolved measurements of gas-phase organic compounds, *Atmos. Meas. Tech.*, **10**, 4687–4696, <https://doi.org/10.5194/amt-10-4687-2017>, 2017.
- Palm, B. B., Liu, X., Jimenez, J. L., and Thornton, J. A.: Performance of a new coaxial ion-molecule reaction region for low-pressure chemical ionization mass spectrometry with reduced instrument wall interactions, *Atmos. Meas. Tech.*, **12**, 5829–5844, <https://doi.org/10.5194/amt-12-5829-2019>, 2019.

- Palm, B. B., Peng, Q., Fredrickson, C. D., Lee, B. H., Garofalo, L. A., Pothier, M. A., Kreidenweis, S. M., Farmer, D. K., Pokhrel, R. P., Shen, Y., Murphy, S. M., Permar, W., Hu, L., Campos, T. L., Hall, S. R., Ullmann, K., Zhang, X., Flocke, F., Fischer, E. V., and Thornton, J. A.: Quantification of organic aerosol and brown carbon evolution in fresh wildfire plumes, *P. Natl. Acad. Sci. USA*, 117, 29469–29477, <https://doi.org/10.1073/pnas.2012218117>, 2020.
- Peng, Q., Palm, B. B., Fredrickson, C. D., Lee, B. H., Hall, S. R., Ullmann, K., Campos, T., Weinheimer, A. J., Apel, E. C., Flocke, F., Permar, W., Hu, L., Garofalo, L. A., Pothier, M. A., Farmer, D. K., Ku, I. T., Sullivan, A. P., Collett, J. L., Fischer, E., and Thornton, J. A.: Observations and Modeling of NO<sub>x</sub> Photochemistry and Fate in Fresh Wildfire Plumes, *ACS Earth Space Chem.*, 5, 2652–2667, <https://doi.org/10.1021/acsearthspacechem.1c00086>, 2021.
- Perring, A. E., Pusede, S. E., and Cohen, R. C.: An observational perspective on the atmospheric impacts of alkyl and multifunctional nitrates on ozone and secondary organic aerosol, *Chem. Rev.*, 113, 5848–5870, <https://doi.org/10.1021/cr300520x>, 2013.
- Pospisilova, V., Lopez-Hilfiker, F. D., Bell, D. M., Haddad, I. E., Mohr, C., Huang, W., Heikkinen, L., Xiao, M., Dommen, J., Prevot, A. S. H., Baltensperger, U., and Slowik, J. G.: On the fate of oxygenated organic molecules in atmospheric aerosol particles, *Sci. Adv.*, 6, eaax8922, <https://doi.org/10.1126/sciadv.aax8922>, 2020.
- Pye, H. O., Luecken, D. J., Xu, L., Boyd, C. M., Ng, N. L., Baker, K. R., Ayres, B. R., Bash, J. O., Baumann, K., Carter, W. P., Edgerton, E., Fry, J. L., Hutzell, W. T., Schwede, D. B., and Shepson, P. B.: Modeling the Current and Future Roles of Particulate Organic Nitrates in the Southeastern United States, *Environ. Sci. Technol.*, 49, 14195–14203, <https://doi.org/10.1021/acs.est.5b03738>, 2015.
- Pye, H. O. T., D'Ambro, E. L., Lee, B. H., Schobesberger, S., Takeuchi, M., Zhao, Y., Lopez-Hilfiker, F., Liu, J., Shilling, J. E., Xing, J., Mathur, R., Middlebrook, A. M., Liao, J., Welti, A., Graus, M., Warneke, C., de Gouw, J. A., Holloway, J. S., Ryrson, T. B., Pollack, I. B., and Thornton, J. A.: Anthropogenic enhancements to production of highly oxygenated molecules from autoxidation, *P. Natl. Acad. Sci. USA*, 116, 6641–6646, <https://doi.org/10.1073/pnas.1810774116>, 2019.
- Reeves, C. E., Mills, G. P., Whalley, L. K., Acton, W. J. F., Bloss, W. J., Crilley, L. R., Grimmond, S., Heard, D. E., Hewitt, C. N., Hopkins, J. R., Kotthaus, S., Kramer, L. J., Jones, R. L., Lee, J. D., Liu, Y., Ouyang, B., Slater, E., Squires, F., Wang, X., Woodward-Massey, R., and Ye, C.: Observations of speciated isoprene nitrates in Beijing: implications for isoprene chemistry, *Atmos. Chem. Phys.*, 21, 6315–6330, <https://doi.org/10.5194/acp-21-6315-2021>, 2021.
- Robinson, M. A., Neuman, J. A., Huey, L. G., Roberts, J. M., Brown, S. S., and Veres, P. R.: Temperature-dependent sensitivity of iodide chemical ionization mass spectrometers, *Atmos. Meas. Tech.*, 15, 4295–4305, <https://doi.org/10.5194/amt-15-4295-2022>, 2022.
- Rollins, A. W., Smith, J. D., Wilson, K. R., and Cohen, R. C.: Real Time In Situ Detection of Organic Nitrates in Atmospheric Aerosols, *Environ. Sci. Technol.*, 44, 5540–5545, <https://doi.org/10.1021/es100926x>, 2010.
- Rollins, A. W., Browne, E. C., Min, K. E., Pusede, S. E., Wooldridge, P. J., Gentner, D. R., Goldstein, A. H., Liu, S., Day, D. A., Russell, L. M., and Cohen, R. C.: Evidence for NO<sub>x</sub> control over nighttime SOA formation, *Science*, 337, 1210–1212, <https://doi.org/10.1126/science.1221520>, 2012.
- Romer, P. S., Duffey, K. C., Wooldridge, P. J., Allen, H. M., Ayres, B. R., Brown, S. S., Brune, W. H., Crouse, J. D., de Gouw, J., Draper, D. C., Feiner, P. A., Fry, J. L., Goldstein, A. H., Koss, A., Misztal, P. K., Nguyen, T. B., Olson, K., Teng, A. P., Wennberg, P. O., Wild, R. J., Zhang, L., and Cohen, R. C.: The lifetime of nitrogen oxides in an isoprene-dominated forest, *Atmos. Chem. Phys.*, 16, 7623–7637, <https://doi.org/10.5194/acp-16-7623-2016>, 2016.
- Romer Present, P. S., Zare, A., and Cohen, R. C.: The changing role of organic nitrates in the removal and transport of NO<sub>x</sub>, *Atmos. Chem. Phys.*, 20, 267–279, <https://doi.org/10.5194/acp-20-267-2020>, 2020.
- Sadanaga, Y., Takagi, R., Ishiyama, A., Nakajima, K., Matsuki, A., and Bandow, H.: Thermal dissociation cavity attenuated phase shift spectroscopy for continuous measurement of total peroxy and organic nitrates in the clean atmosphere, *Rev. Sci. Instr.*, 87, 074102, <https://doi.org/10.1063/1.4958167>, 2016.
- Salvador, C. M. G., Tang, R., Priestley, M., Li, L., Tsiligiannis, E., Le Breton, M., Zhu, W., Zeng, L., Wang, H., Yu, Y., Hu, M., Guo, S., and Hallquist, M.: Ambient nitro-aromatic compounds – biomass burning versus secondary formation in rural China, *Atmos. Chem. Phys.*, 21, 1389–1406, <https://doi.org/10.5194/acp-21-1389-2021>, 2021.
- Schobesberger, S., D'Ambro, E. L., Lopez-Hilfiker, F. D., Mohr, C., and Thornton, J. A.: A model framework to retrieve thermodynamic and kinetic properties of organic aerosol from composition-resolved thermal desorption measurements, *Atmos. Chem. Phys.*, 18, 14757–14785, <https://doi.org/10.5194/acp-18-14757-2018>, 2018.
- Shen, H., Zhao, D., Pullinen, I., Kang, S., Vereecken, L., Fuchs, H., Acir, I. H., Tillmann, R., Rohrer, F., Wildt, J., Kiendler-Scharr, A., Wahner, A., and Mentel, T. F.: Highly Oxygenated Organic Nitrates Formed from NO<sub>3</sub> Radical-Initiated Oxidation of beta-Pinene, *Environ. Sci. Technol.*, 55, 15658–15671, <https://doi.org/10.1021/acs.est.1c03978>, 2021.
- Simoneit, B. R. T.: Biomass burning – a review of organic tracers for smoke from incomplete combustion, *Appl. Geochem.*, 17, 129–162, [https://doi.org/10.1016/S0883-2927\(01\)00061-0](https://doi.org/10.1016/S0883-2927(01)00061-0), 2002.
- Simoneit, B. R. T., Schauer, J. J., Nolte, C. G., Oros, D. R., Elias, V. O., Fraser, M. P., Rogge, W. F., and Cass, G. R.: Levoglucosan, a tracer for cellulose in biomass burning and atmospheric particles, *Atmos. Environ.*, 33, 173–182, [https://doi.org/10.1016/S1352-2310\(98\)00145-9](https://doi.org/10.1016/S1352-2310(98)00145-9), 1999.
- Sobanski, N., Thieser, J., Schuladen, J., Sauvage, C., Song, W., Williams, J., Lelieveld, J., and Crowley, J. N.: Day and nighttime formation of organic nitrates at a forested mountain site in south-west Germany, *Atmos. Chem. Phys.*, 17, 4115–4130, <https://doi.org/10.5194/acp-17-4115-2017>, 2017.
- Song, K., Guo, S., Wang, H., Yu, Y., Wang, H., Tang, R., Xia, S., Gong, Y., Wan, Z., Lv, D., Tan, R., Zhu, W., Shen, R., Li, X., Yu, X., Chen, S., Zeng, L., and Huang, X.: Measurement report: Online measurement of gas-phase nitrated phenols utilizing a CI-LToF-MS: primary sources and secondary formation, At-

- mos. Chem. Phys., 21, 7917–7932, <https://doi.org/10.5194/acp-21-7917-2021>, 2021.
- Takeuchi, M. and Ng, N. L.: Chemical composition and hydrolysis of organic nitrate aerosol formed from hydroxyl and nitrate radical oxidation of  $\alpha$ -pinene and  $\beta$ -pinene, *Atmos. Chem. Phys.*, 19, 12749–12766, <https://doi.org/10.5194/acp-19-12749-2019>, 2019.
- Thornton, J. A., Mohr, C., Schobesberger, S., D'Ambro, E. L., Lee, B. H., and Lopez-Hilfiker, F. D.: Evaluating Organic Aerosol Sources and Evolution with a Combined Molecular Composition and Volatility Framework Using the Filter Inlet for Gases and Aerosols (FIGAERO), *Acc. Chem. Res.*, 53, 1415–1426, <https://doi.org/10.1021/acs.accounts.0c00259>, 2020.
- Turpin, B. J. and Huntzicker, J. J.: Identification of secondary organic aerosol episodes and quantitation of primary and secondary organic aerosol concentrations during SCAQS, *Atmos. Environ.*, 29, 3527–3544, [https://doi.org/10.1016/1352-2310\(94\)00276-Q](https://doi.org/10.1016/1352-2310(94)00276-Q), 1995.
- Wang, C., Yuan, B., Wu, C., Wang, S., Qi, J., Wang, B., Wang, Z., Hu, W., Chen, W., Ye, C., Wang, W., Sun, Y., Wang, C., Huang, S., Song, W., Wang, X., Yang, S., Zhang, S., Xu, W., Ma, N., Zhang, Z., Jiang, B., Su, H., Cheng, Y., Wang, X., and Shao, M.: Measurements of higher alkanes using  $\text{NO}^+$  chemical ionization in PTR-ToF-MS: important contributions of higher alkanes to secondary organic aerosols in China, *Atmos. Chem. Phys.*, 20, 14123–14138, <https://doi.org/10.5194/acp-20-14123-2020>, 2020.
- Wang, L., Wu, D., and Zhang, Z.: Characterization of typical biomass burning tracers among atmospheric particles in urban Guangzhou, *J. Grad. Univ. Chin. Acad. Sci.*, 34, 567–572, <https://doi.org/10.7523/j.issn.2095-6134.2017.05.006>, 2017.
- Wang, L., Wang, X., Gu, R., Wang, H., Yao, L., Wen, L., Zhu, F., Wang, W., Xue, L., Yang, L., Lu, K., Chen, J., Wang, T., Zhang, Y., and Wang, W.: Observations of fine particulate nitrated phenols in four sites in northern China: concentrations, source apportionment, and secondary formation, *Atmos. Chem. Phys.*, 18, 4349–4359, <https://doi.org/10.5194/acp-18-4349-2018>, 2018.
- Wang, M., Chen, D., Xiao, M., Ye, Q., Stolzenburg, D., Hofbauer, V., Ye, P., Vogel, A. L., Mauldin, R. L., 3rd, Amorim, A., Baccarini, A., Baumgartner, B., Brikkle, S., Dada, L., Dias, A., Duplissy, J., Finkenzeller, H., Garmash, O., He, X. C., Hoyle, C. R., Kim, C., Kvashnin, A., Lehtipalo, K., Fischer, L., Molteni, U., Petaja, T., Pospisilova, V., Quelever, L. L. J., Rissanen, M., Simon, M., Tauber, C., Tome, A., Wagner, A. C., Weitz, L., Volkamer, R., Winkler, P. M., Kirkby, J., Worsnop, D. R., Kulmala, M., Baltensperger, U., Dommen, J., El-Haddad, I., and Donahue, N. M.: Photo-oxidation of Aromatic Hydrocarbons Produces Low-Volatility Organic Compounds, *Environ. Sci. Technol.*, 54, 7911–7921, <https://doi.org/10.1021/acs.est.0c02100>, 2020.
- Wang, S. and Li, H.:  $\text{NO}_3^-$ -Initiated Gas-Phase Formation of Nitrated Phenolic Compounds in Polluted Atmosphere, *Environ. Sci. Technol.*, 55, 2899–2907, <https://doi.org/10.1021/acs.est.0c08041>, 2021.
- Wang, S., Peng, Y., Peng, Q., Wu, C., Wang, C., Wang, B., Wang, Z., Kuang, Y., Song, W., Wang, X., Hu, W., Chen, W., Shen, J., Chen, D., Shao, M., and Yuan, B.: Different chemical removal pathways of volatile organic compounds (VOCs): Comparison of urban and regional sites, *Acta Sci. Circumstantiae*, 40, 2311–2322, <https://doi.org/10.13671/j.hjkxxb.2020.0153>, 2020.
- Wang, S., Yuan, B., Wu, C., Wang, C., Li, T., He, X., Huangfu, Y., Qi, J., Li, X.-B., Sha, Q., Zhu, M., Lou, S., Wang, H., Karl, T., Graus, M., Yuan, Z., and Shao, M.: Oxygenated volatile organic compounds (VOCs) as significant but varied contributors to VOC emissions from vehicles, *Atmos. Chem. Phys.*, 22, 9703–9720, <https://doi.org/10.5194/acp-22-9703-2022>, 2022.
- Wang, Y., Hu, M., Lin, P., Guo, Q., Wu, Z., Li, M., Zeng, L., Song, Y., Zeng, L., Wu, Y., Guo, S., Huang, X., and He, L.: Molecular Characterization of Nitrogen-Containing Organic Compounds in Humic-like Substances Emitted from Straw Residue Burning, *Environ. Sci. Technol.*, 51, 5951–5961, <https://doi.org/10.1021/acs.est.7b00248>, 2017.
- Wang, Y., Hu, M., Lin, P., Tan, T., Li, M., Xu, N., Zheng, J., Du, Z., Qin, Y., Wu, Y., Lu, S., Song, Y., Wu, Z., Guo, S., Zeng, L., Huang, X., and He, L.: Enhancement in Particulate Organic Nitrogen and Light Absorption of Humic-Like Substances over Tibetan Plateau Due to Long-Range Transported Biomass Burning Emissions, *Environ. Sci. Technol.*, 53, 14222–14232, <https://doi.org/10.1021/acs.est.9b06152>, 2019.
- Wang, Z., Yuan, B., Ye, C., Roberts, J., Wisthaler, A., Lin, Y., Li, T., Wu, C., Peng, Y., Wang, C., Wang, S., Yang, S., Wang, B., Qi, J., Wang, C., Song, W., Hu, W., Wang, X., Xu, W., Ma, N., Kuang, Y., Tao, J., Zhang, Z., Su, H., Cheng, Y., Wang, X., and Shao, M.: High Concentrations of Atmospheric Isocyanic Acid (HNCO) Produced from Secondary Sources in China, *Environ. Sci. Technol.*, 54, 11818–11826, <https://doi.org/10.1021/acs.est.0c02843>, 2020.
- Wang, Z., Shi, Z., Wang, F., Liang, W., Shi, G., Wang, W., Chen, D., Liang, D., Feng, Y., and Russell, A. G.: Implications for ozone control by understanding the survivor bias in observed ozone-volatile organic compounds system, *npj Climate and Atmospheric Science*, 5, 39, <https://doi.org/10.1038/s41612-022-00261-7>, 2022.
- WaveMetrics: Igor Pro from WaveMetrics, <https://www.wavemetrics.com>, last access: 1 January 2023.
- Wennberg, P. O., Bates, K. H., Crouse, J. D., Dodson, L. G., McVay, R. C., Mertens, L. A., Nguyen, T. B., Praske, E., Schwantes, R. H., Smarte, M. D., St Clair, J. M., Teng, A. P., Zhang, X., and Seinfeld, J. H.: Gas-Phase Reactions of Isoprene and Its Major Oxidation Products, *Chem. Rev.*, 118, 3337–3390, <https://doi.org/10.1021/acs.chemrev.7b00439>, 2018.
- Wolfe, G. M., Marvin, M. R., Roberts, S. J., Travis, K. R., and Liao, J.: The Framework for 0-D Atmospheric Modeling (F0AM) v3.1, *Geosci. Model Dev.*, 9, 3309–3319, <https://doi.org/10.5194/gmd-9-3309-2016>, 2016.
- Wormhoudt, J., Wood, E. C., Knighton, W. B., Kolb, C. E., Herndon, S. C., and Olaguer, E. P.: Vehicle emissions of radical precursors and related species observed in the 2009 SHARP campaign, *J. Air Waste Manage. Assoc.*, 65, 699–706, <https://doi.org/10.1080/10962247.2015.1008654>, 2015.
- Wu, C., Bell, D. M., Graham, E. L., Haslett, S., Riipinen, I., Baltensperger, U., Bertrand, A., Giannoukos, S., Schoonbaert, J., El Haddad, I., Prevot, A. S. H., Huang, W., and Mohr, C.: Photolytically induced changes in composition and volatility of biogenic secondary organic aerosol from nitrate radical oxidation during night-to-day transition, *Atmos. Chem. Phys.*, 21, 14907–14925, <https://doi.org/10.5194/acp-21-14907-2021>, 2021.
- Wu, C., Wang, C., Wang, S., Wang, W., Yuan, B., Qi, J., Wang, B., Wang, H., Wang, C., Song, W., Wang, X., Hu, W., Lou,

- S., Ye, C., Peng, Y., Wang, Z., Huangfu, Y., Xie, Y., Zhu, M., Zheng, J., Wang, X., Jiang, B., Zhang, Z., and Shao, M.: Measurement report: Important contributions of oxygenated compounds to emissions and chemistry of volatile organic compounds in urban air, *Atmos. Chem. Phys.*, 20, 14769–14785, <https://doi.org/10.5194/acp-20-14769-2020>, 2020.
- Xiao, S. and Bertram, A. K.: Reactive uptake kinetics of  $\text{NO}_3$  on multicomponent and multiphase organic mixtures containing unsaturated and saturated organics, *Phys. Chem. Chem. Phys.*, 13, 6628–6636, <https://doi.org/10.1039/C0CP02682D>, 2011.
- Xu, L., Suresh, S., Guo, H., Weber, R. J., and Ng, N. L.: Aerosol characterization over the southeastern United States using high-resolution aerosol mass spectrometry: spatial and seasonal variation of aerosol composition and sources with a focus on organic nitrates, *Atmos. Chem. Phys.*, 15, 7307–7336, <https://doi.org/10.5194/acp-15-7307-2015>, 2015.
- Xu, L., Crounse, J. D., Vasquez, K. T., Allen, H., Wennberg, P. O., Bourgeois, I., Brown, S. S., Campuzano-Jost, P., Coggon, M. M., Crawford, J. H., DiGangi, J. P., Diskin, G. S., Fried, A., Gargulinski, E. M., Gilman, J. B., Gkatzelis, G. I., Guo, H., Hair, J. W., Hall, S. R., Halliday, H. A., Hanisco, T. F., Hannun, R. A., Holmes, C. D., Huey, L. G., Jimenez, J. L., Lamplugh, A., Lee, Y. R., Liao, J., Lindaas, J., Neuman, J. A., Nowak, J. B., Peischl, J., Peterson, D. A., Piel, F., Richter, D., Rickly, P. S., Robinson, M. A., Rollins, A. W., Ryerson, T. B., Sekimoto, K., Selimovic, V., Shingler, T., Soja, A. J., St. Clair, J. M., Tanner, D. J., Ullmann, K., Veres, P. R., Walega, J., Warneke, C., Washenfelder, R. A., Weibring, P., Wisthaler, A., Wolfe, G. M., Womack, C. C., and Yokelson, R. J.: Ozone chemistry in western U.S. wildfire plumes, *Sci. Adv.*, 7, eabl3648, <https://doi.org/10.1126/sciadv.abl3648>, 2021.
- Xu, W., Takeuchi, M., Chen, C., Qiu, Y., Xie, C., Xu, W., Ma, N., Worsnop, D. R., Ng, N. L., and Sun, Y.: Estimation of particulate organic nitrates from thermodenuder–aerosol mass spectrometer measurements in the North China Plain, *Atmos. Meas. Tech.*, 14, 3693–3705, <https://doi.org/10.5194/amt-14-3693-2021>, 2021.
- Ye, C., Yuan, B., Lin, Y., Wang, Z., Hu, W., Li, T., Chen, W., Wu, C., Wang, C., Huang, S., Qi, J., Wang, B., Wang, C., Song, W., Wang, X., Zheng, E., Krechmer, J. E., Ye, P., Zhang, Z., Wang, X., Worsnop, D. R., and Shao, M.: Chemical characterization of oxygenated organic compounds in the gas phase and particle phase using iodide CIMS with FIGAERO in urban air, *Atmos. Chem. Phys.*, 21, 8455–8478, <https://doi.org/10.5194/acp-21-8455-2021>, 2021.
- Yu, K., Zhu, Q., Du, K., and Huang, X.-F.: Characterization of nighttime formation of particulate organic nitrates based on high-resolution aerosol mass spectrometry in an urban atmosphere in China, *Atmos. Chem. Phys.*, 19, 5235–5249, <https://doi.org/10.5194/acp-19-5235-2019>, 2019.
- Yuan, B., Liu, Y., Shao, M., Lu, S., and Streets, D. G.: Biomass Burning Contributions to Ambient VOCs Species at a Receptor Site in the Pearl River Delta (PRD), China, *Environ. Sci. Technol.*, 44, 4577–4582, <https://doi.org/10.1021/es1003389>, 2010.
- Yuan, B., Hu, W. W., Shao, M., Wang, M., Chen, W. T., Lu, S. H., Zeng, L. M., and Hu, M.: VOC emissions, evolutions and contributions to SOA formation at a receptor site in eastern China, *Atmos. Chem. Phys.*, 13, 8815–8832, <https://doi.org/10.5194/acp-13-8815-2013>, 2013.
- Yuan, B., Koss, A. R., Warneke, C., Coggon, M., Sekimoto, K., and de Gouw, J. A.: Proton-Transfer-Reaction Mass Spectrometry: Applications in Atmospheric Sciences, *Chem. Rev.*, 117, 13187–13229, <https://doi.org/10.1021/acs.chemrev.7b00325>, 2017.
- Zhang, J. K., Cheng, M. T., Ji, D. S., Liu, Z. R., Hu, B., Sun, Y., and Wang, Y. S.: Characterization of submicron particles during biomass burning and coal combustion periods in Beijing, China, *Sci. Total Environ.*, 562, 812–821, <https://doi.org/10.1016/j.scitotenv.2016.04.015>, 2016.
- Zhao, Y., Nguyen, N. T., Presto, A. A., Hennigan, C. J., May, A. A., and Robinson, A. L.: Intermediate Volatility Organic Compound Emissions from On-Road Gasoline Vehicles and Small Off-Road Gasoline Engines, *Environ. Sci. Technol.*, 50, 4554–4563, <https://doi.org/10.1021/acs.est.5b06247>, 2016.
- Zhao, Y., Thornton, J. A., and Pye, H. O. T.: Quantitative constraints on autoxidation and dimer formation from direct probing of monoterpene-derived peroxy radical chemistry, *P. Natl. Acad. Sci. USA*, 115, 12142–12147, <https://doi.org/10.1073/pnas.1812147115>, 2018.
- Zhao, Z., Husainy, S., Stoudemayer, C. T., and Smith, G. D.: Reactive uptake of  $\text{NO}_3$  radicals by unsaturated fatty acid particles, *Phys. Chem. Chem. Phys.*, 13, 17809–17817, <https://doi.org/10.1039/c1cp21790a>, 2011.